SUPPORTING INFORMATION

Development of the first panchromatic BODPIY-based one-component iodonium salts for initiating the photopolymerization processes

Monika Topa, [1] Mariusz Galek, [2] Magdalena Jankowska, [1] Fabrice Morlet-Savary, [3] Bernadette Graff, [3] Jacques Lalevée, [3] Roman Popielarz [1] and Joanna Ortyl [1,2*]

[1] Department of Biotechnology and Physical Chemistry, Faculty of Chemical Engineering and Technology, Cracow University of Technology, Warszawska 24, 31-155 Cracow, Poland

[2] Photo HiTech Ltd., Bobrzyńskiego 14, 30-348 Cracow, Poland

[3] Institut de Science des Matériaux de Mulhouse IS2M, UMR CNRS 7361, UHA, 15, rue Jean Starcky, Cedex 68057 Mulhouse, France

* Corresponding author: Joanna Ortyl

e- mail: jortyl@pk.edu.pl

ORCID iD: 0000-0002-4789-7199

Synthesis - chemicals and general synthetic procedures of iodonium salts

Structural formulas of new iodonium salts which were synthesized following the published procedure[1] and were presented in Table S1. Procedure synthesis and synthetic scheme are shown in Scheme 1.

1. Synthesis of 4,4-difluoro-1,3,5,7,8-pentametylo-4-bora-3a, 4a-diaza-s-indacen (**B-1**)

To 2,4-dimethylpyrrole (21mmol) dissolved in dichloromethane (8cm^3) under argon, acetyl chloride (49mmol) was added dropwise over 30 min at room temperature, hexane (40cm^3) was successively added and the mixture was evaporated to dryness. The residue was dissolved in dichloromethane (97cm^3), triethylamine (61mmol) was added and the mixture was stirred for 10 min at room temperature under argon. After that, boron trifluoride diethyl ether (262mmol) was added and the mixture was further stirred for 1h at room temperature. The progress of the reaction was monitored by thin layer chromatography (TLC). The reaction mixture was washed with aqueous sodium bicarbonate ($NaHCO_3$) and dried over sodium sulfate (Na_2SO_4), concentrated and crystallized from ethyl acetate.

2. Synthesis of tosylate phenyl[4,4-difluoro-1,3,5,7,8-pentametylo-4-bora-3a, 4a-diaza-s-indacene]iodonium (**B-IOD-TsO**)

4,4-difluoro-1,3,5,7,8-pentametylo-4-bora-3a, 4a-diaza-s-indacen (B-1) (3.8mmol) and hydroxy-tosyloxy-iodobenzene (HTIB) (1.9mmol) were dissolved in chloroform (30ml) and the mixture was stirred overnight at the reflux temperature of the solvent. The progress of the reaction was monitored by thin layer chromatography (TLC). It was evaporated to dryness. Then, the residue was dissolved in dichloromethane (DCM) and acetone (1: 1). The organic phase was washed with distilled water, dried over sodium sulfate (VI). The solvent was evaporated. The product was purified using the flash column (eluent DCM → DCM / MeOH 4:).

3. Synthesis of the remaining iodonium salts (**B-IOD-PF_6, B-IOD-SbF_6, B-IOD-CF_3SO_3**)

The **B-IOD-TsO** (1.6 mmol) was then dissolved in dichloromethane (DCM) and acetone (1:1). Then the appropriate salt : KPF_6, $NaSbF_6$, CF_3SO_3K (1.7 mmol) was added in an acetone solution (15ml), and the mixture was stirred for 30 min at room temperature. Water (50 ml) was added and the mixture was stirred for 30 min. The resulting precipitate was filtered off, washed with distilled water, dried over sodium sulfate, the solvent was evaporated. The product was purified on a flash column (eluent dichloromethane → dichloromethane / methanol 4:1).

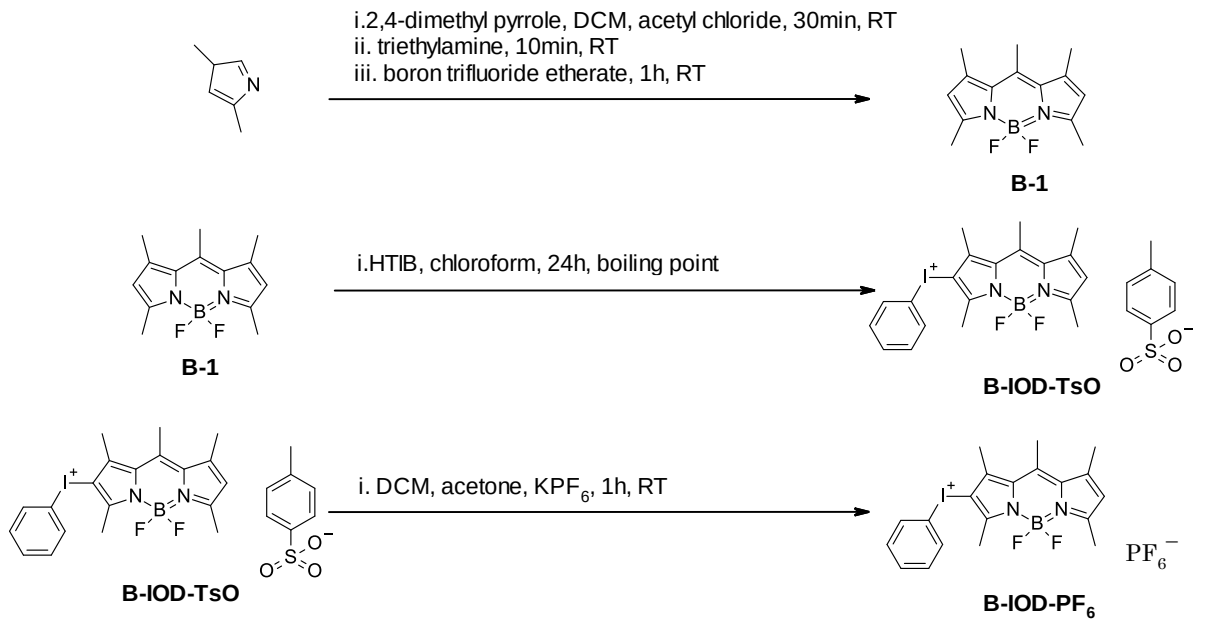

Scheme S1. Synthetic scheme of BODIPY derivatives.

All inorganic salts organic reagents, and solvents were analytically pure and used as received. Structure and purity of obtained products were confirmed by NMR and LC–MS analysis. ^{1}H and ^{13}CNMR spectra were recorded in DMSO–D_6 on Avance III HD 400 MHz (Bruker) spectrometer. Chemical shifts were reported in parts per million (δ) and referenced to residual protonated solvent peak (δ=2.50 ppm in ^{1}HNMR spectra and 39.52 ppm ^{13}CNMR spectra.

Table S1. Structures of investigated photoinitiators

New panchromatic one-component iodonium salts		
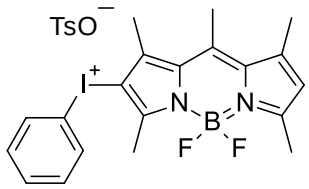	B-IOD-TsO	Tosylate phenyl[4,4-difluoro-1,3,5,7,8-pentametylo-4-bora-3a, 4a-diaza-s-indacene]iodonium
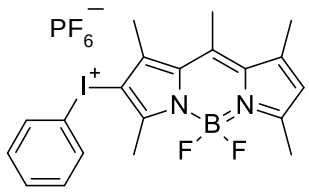	B-IOD-PF_6	Hexafluorophosphate phenyl[4,4-difluoro-1,3,5,7,8-pentametylo-4-bora-3a, 4a-diaza-s-indacene]iodonium
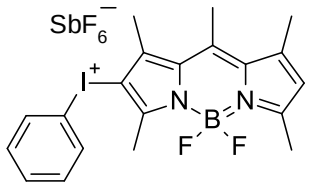	B-IOD-SbF_6	Hexafluoroantimonate phenyl[4,4-difluoro-1,3,5,7,8-pentametylo-4-bora-3a, 4a-diaza-s-indacene]iodonium
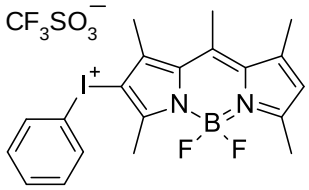	B-IOD-CF_3SO_3	Triflate phenyl[4,4-difluoro-1,3,5,7,8-pentametylo-4-bora-3a, 4a-diaza-s-indacene]iodonium
Bimolecular photoinitiating system		
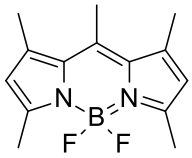	B-1	4,4-difluoro-1,3,5,7,8-pentametylo-4-bora-3a, 4a-diaza-s-indacen
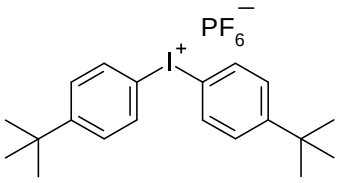	Speedcure 938	Bis-(4-t-butylphenyl)-Iodonium hexafluorophosphate

Tosylate phenyl[4,4-difluoro-1,3,5,7,8-pentametylo-4-bora-3a, 4a-diaza-s-indacene]iodonium, ***B-IOD-TsO***

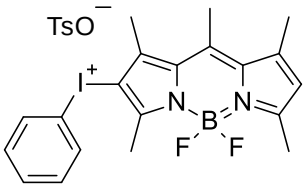

Yield: 0,300 g (32%);

^{1}H NMR (400 MHz, DMSO) δ 8.08 (d, J = 8.5 Hz, 2H), 7.64 (t, *J* = 7.4 Hz, 1H), 7.53 – 7.44 (m, 4H), 7.11 (d, J = 7.8 Hz, 2H), 6.53 (s, 1H), 2.69 (s, 3H), 2.66 (s, 3H), 2.62 (s, 3H), 2.48 (s, 3H), 2.28 (s, 3H), 1.23 (s, 3H).

^{13}C NMR (101 MHz, DMSO) δ 161.29, 150.07, 147.98, 146.24, 144.63, 139.29, 137.99, 134.71,134.61 132.15, 130.02, 130.25, 129.35, 128.66, 128.47, 125.93, 125.22 , 118.60, 21.23, 17.96, 17.81, 17.49, 15.05, 14.91

MS (ESI) m/z(%): 465 ([M+H]$^{+}$, 100%); purity (LC): >95%.

Hexafluorophosphate phenyl[4,4-difluoro-1,3,5,7,8-pentametylo-4-bora-3a, 4a-diaza-s -indacene]iodonium, ***B-IOD-PF$_6$***

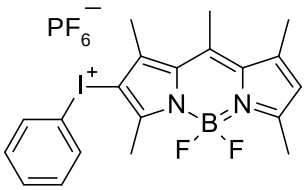

Yield: 1,32 g (36%);

^{1}H NMR (400 MHz, DMSO) δ 8.11 (d, J = 8.3 Hz, 2H), 7.66 (t, J = 7.4 Hz, 1H), 7.53 (t, J = 7.7 Hz, 2H), 6.54 (s, 1H), 2.70 (s, 3H), 2.68 (s, 3H), 2.64 (s, 3H), 2.48 (s, 3H), 1.23 (s, 3H).

^{13}C NMR (101 MHz, DMSO) δ 161.57, 154.30, 149.97, 148.16, 144.65, 139.43, 139.18, 138.35, 134.71, 132.25, 132.20, 130.26, 125.35, 117.95, 17.92, 17.83, 17.50, 15.08, 14.90.

MS (ESI) m/z(%): 465 ([M+H]$^{+}$, 100%); purity (LC): >91%.

Hexafluoroantimonate phenyl[4,4-difluoro-1,3,5,7,8-pentametylo-4-bora-3a, 4a-diaza-s-indacene]iodonium, ***B-IOD-SbF$_6$***

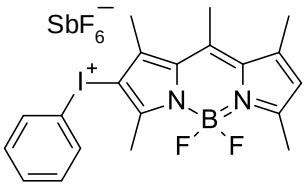

Yield: 0.108 g (26%);

^{1}H NMR (400 MHz, DMSO) δ 8.11 (d, J = 7.4 Hz, 2H), 7.66 (t, J = 7.9 Hz, 1H), 7.53 (t, J = 7.7 Hz, 2H), 6.55 (s, 1H), 2.70 (s, 3H), 2.67 (s, 3H), 2.63 (s, 3H), 2.49 (s, 3H), 1.24 (s, 3H).

^{13}C NMR (101 MHz, DMSO) δ 148.27, 144.65, 139.54, 139.15, 134.83, 134.77, 132.31, 130.27, 128.47, 125.94, 125.40, 124.57, 117.60, 30.85, 29.44, 17.91, 17.84, 17.51, 15.10.

MS (ESI) m/z(%): 465 ([M+H]$^{+}$, 100%); purity (LC): >96%.

Hexafluorophosphate phenyl[4,4-difluoro-1,3,5,7,8-pentametylo-4-bora-3a, 4a-diaza-s -indacene]iodonium , ***B-IOD-CF$_3$SO$_3$***

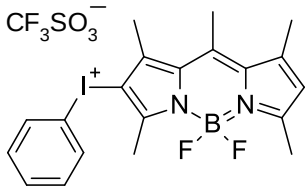

Yield: 0.115 g (28%);

^{1}H NMR (400 MHz, DMSO) δ 8.11 (d, J = 7.4 Hz, 2H), 7.66 (t, J = 7.9 Hz, 1H), 7.53 (t, J = 7.7 Hz, 2H), 6.55 (s, 1H), 2.70 (s, 3H), 2.67 (s, 3H), 2.63 (s, 3H), 2.49 (s, 3H), 1.24 (s, 3H).

^{13}C NMR (101 MHz, DMSO) δ 161.68, 149.96, 148.23, 144.65, 139.16, 134.91, 134.77, 132.30, 130.26, 128.47, 125.92, 125.36, 117.60, 30.84, 29.45, 17.91, 17.82, 17.50, 15.08.

MS (ESI) m/z(%): 465 ([M+H]$^+$, 100%); purity (LC): >96%.

NMR spectra of synthesized iodonium salts

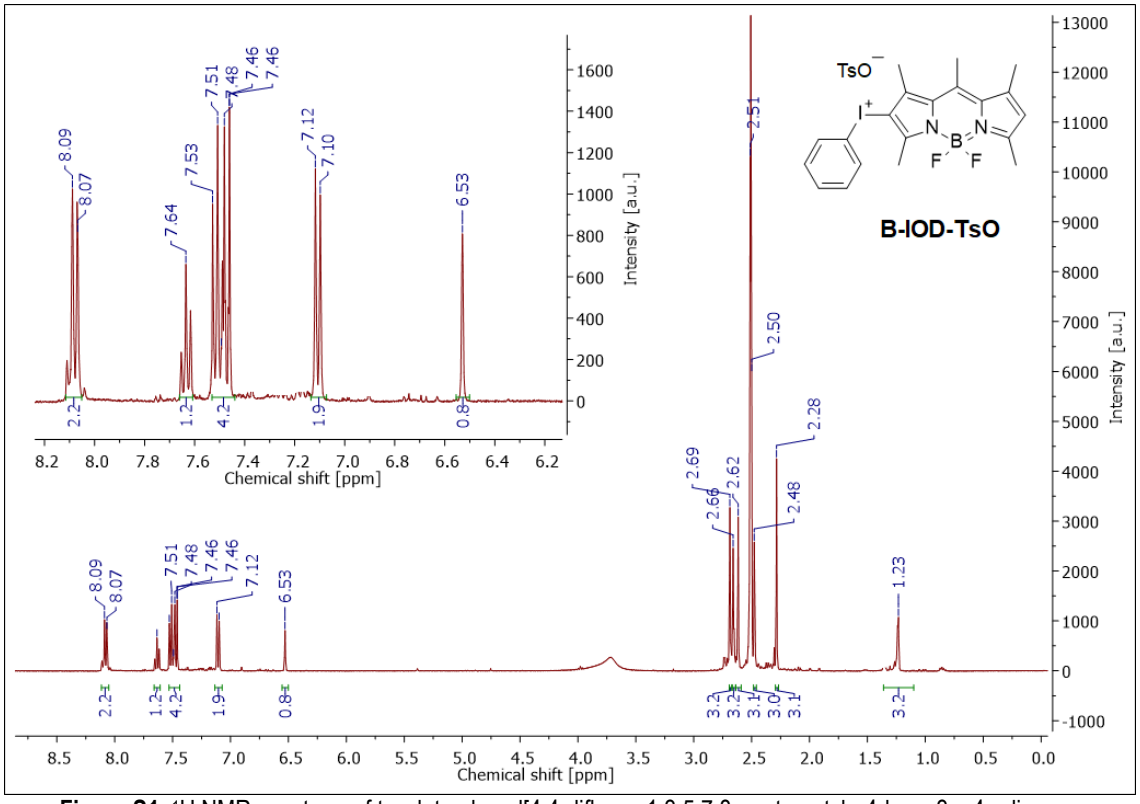

Figure S1. ^{1}H NMR spectrum of tosylate phenyl[4,4-difluoro-1,3,5,7,8-pentametylo-4-bora-3a, 4a-diaza-s-indacene]iodonium.

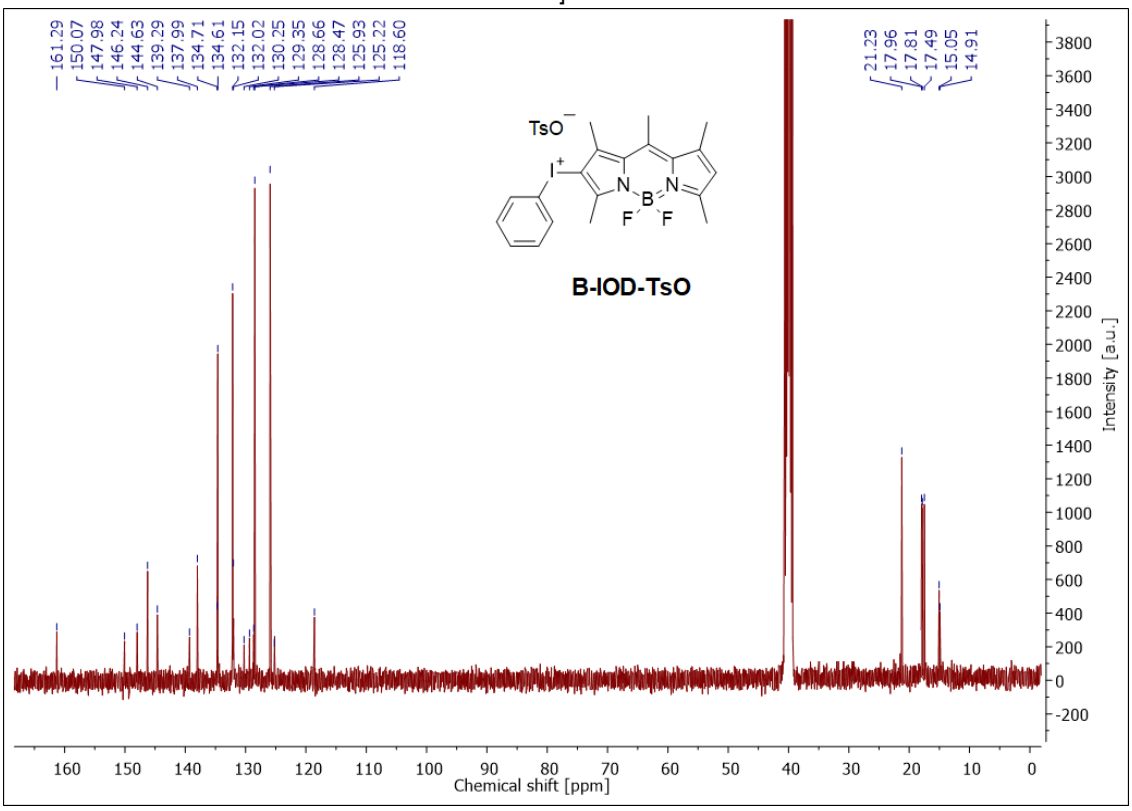

Figure S2. ^{13}C NMR spectrum of tosylate phenyl[4,4-difluoro-1,3,5,7,8-pentametylo-4-bora-3a, 4a-diaza-s-indacene]iodonium.

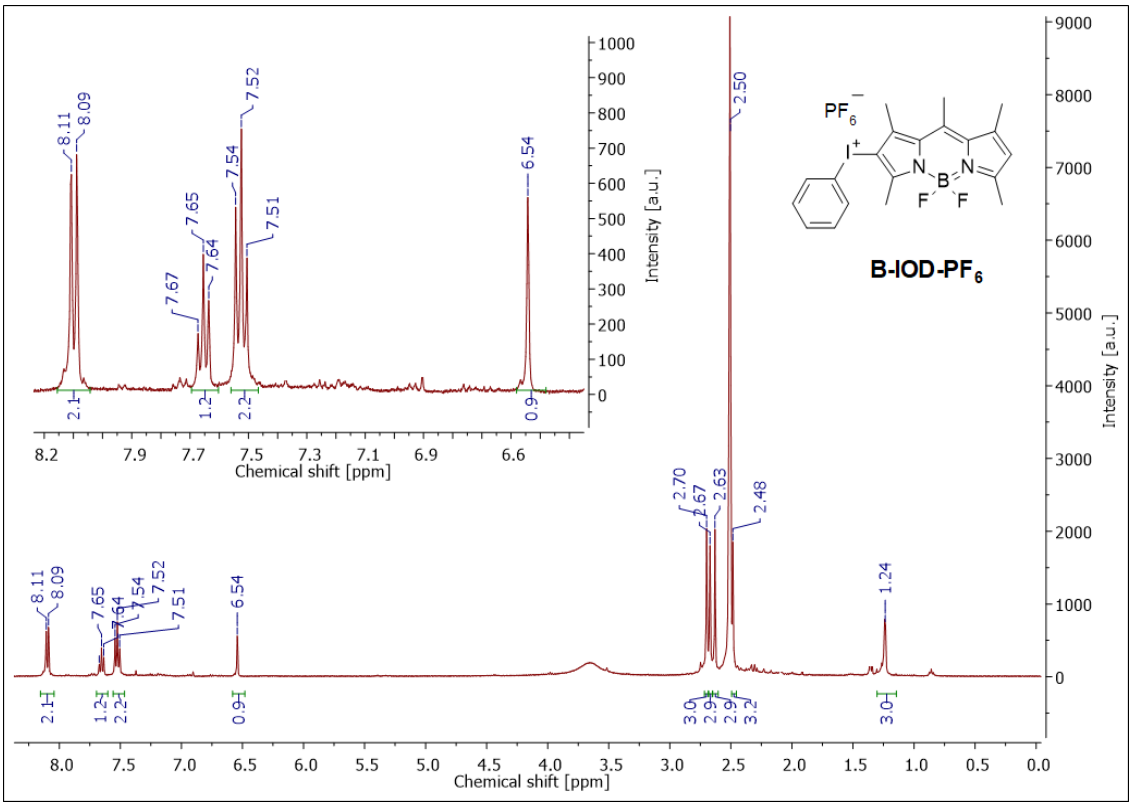

Figure S3. ^{1}H NMR spectrum of hexafluorophosphate phenyl[4,4-difluoro-1,3,5,7,8-pentametylo-4-bora-3a, 4a-diaza-s -indacene]iodonium.

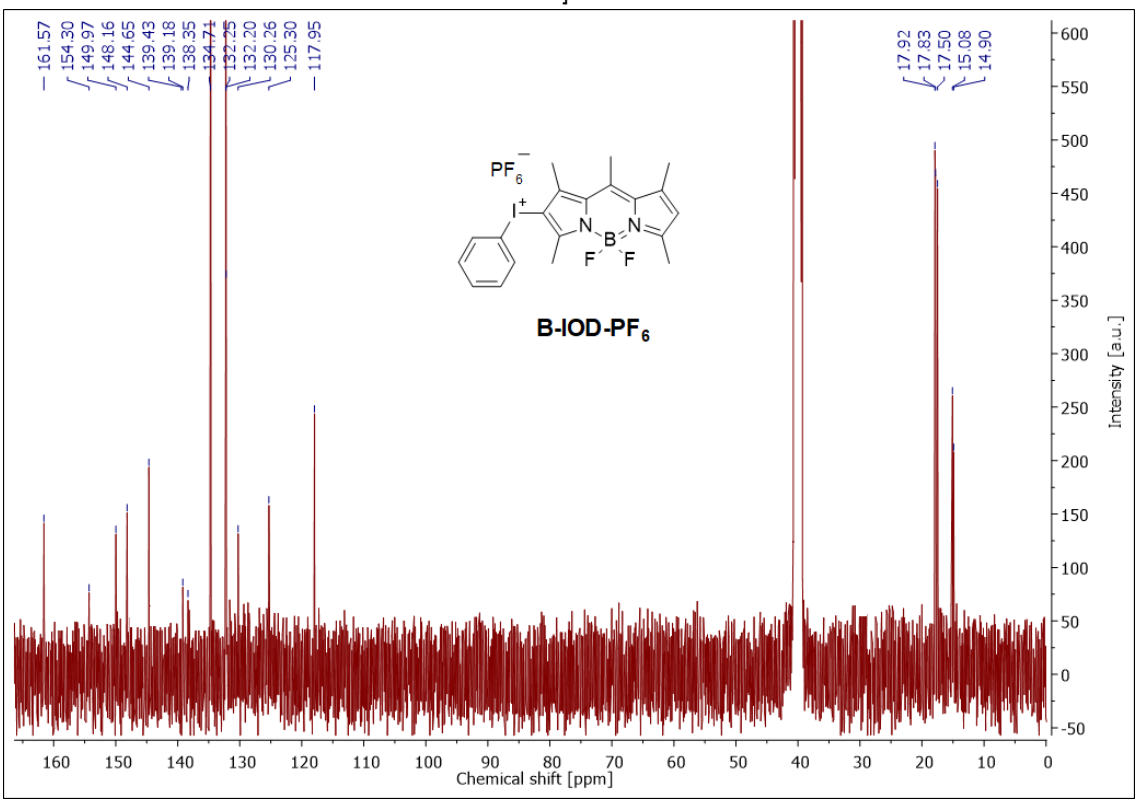

Figure S4. ^{13}C NMR spectrum of hexafluorophosphate phenyl[4,4-difluoro-1,3,5,7,8-pentametylo-4-bora-3a, 4a-diaza-s -indacene]iodonium.

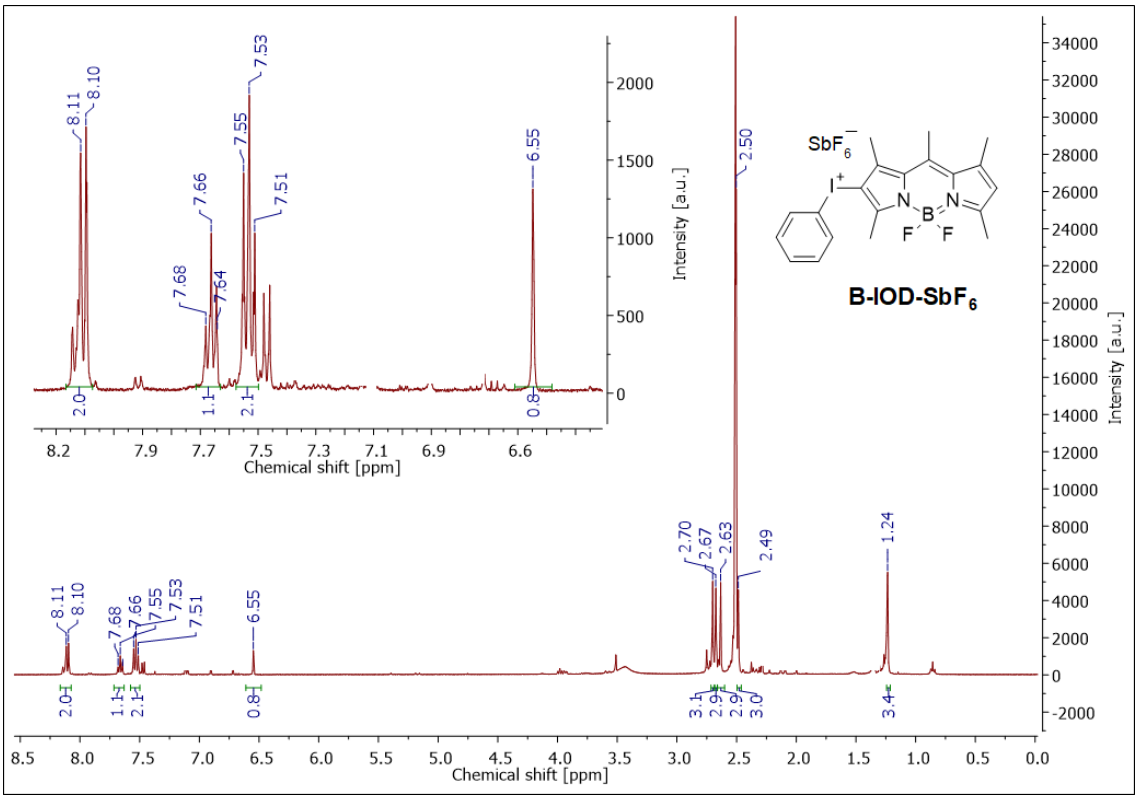

Figure S5. ^{1}H NMR spectrum of hexafluoroantimonate phenyl[4,4-difluoro-1,3,5,7,8-pentametylo-4-bora-3a, 4a-diaza-s-indacene]iodonium.

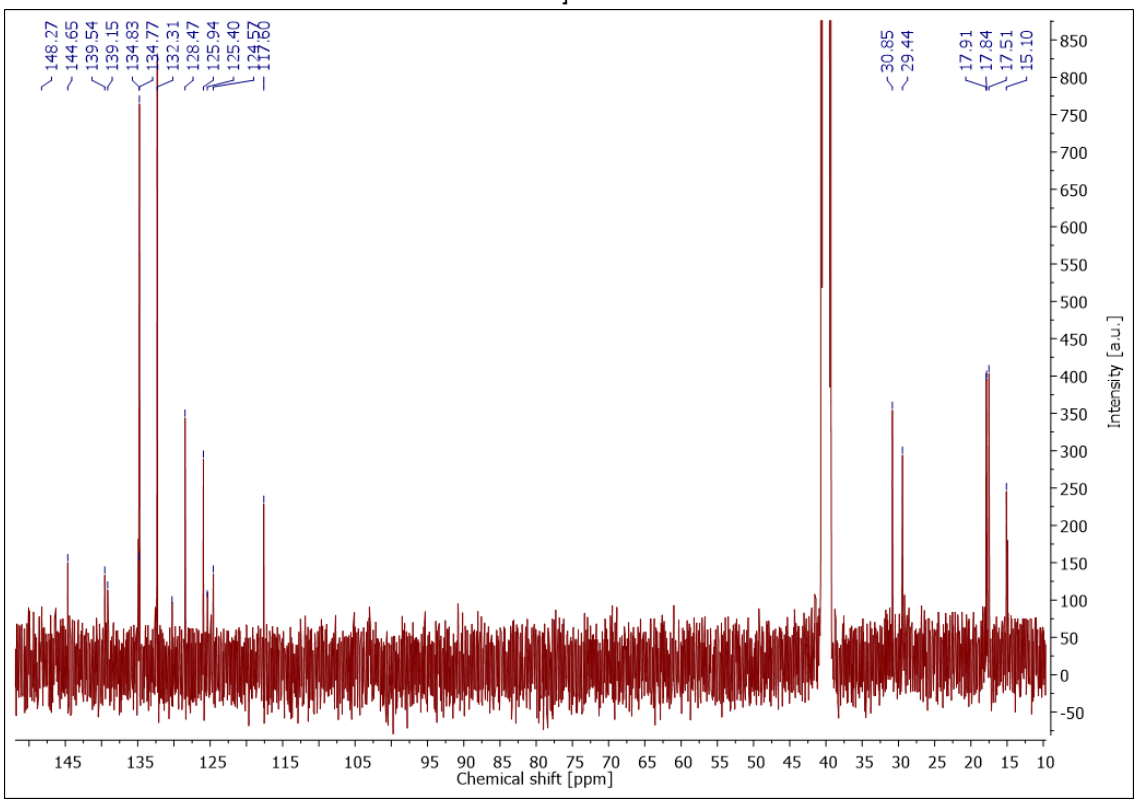

Figure S6. ^{13}C NMR spectrum of hexafluoroantimonate phenyl[4,4-difluoro-1,3,5,7,8-pentametylo-4-bora-3a, 4a-diaza-s-indacene]iodonium.

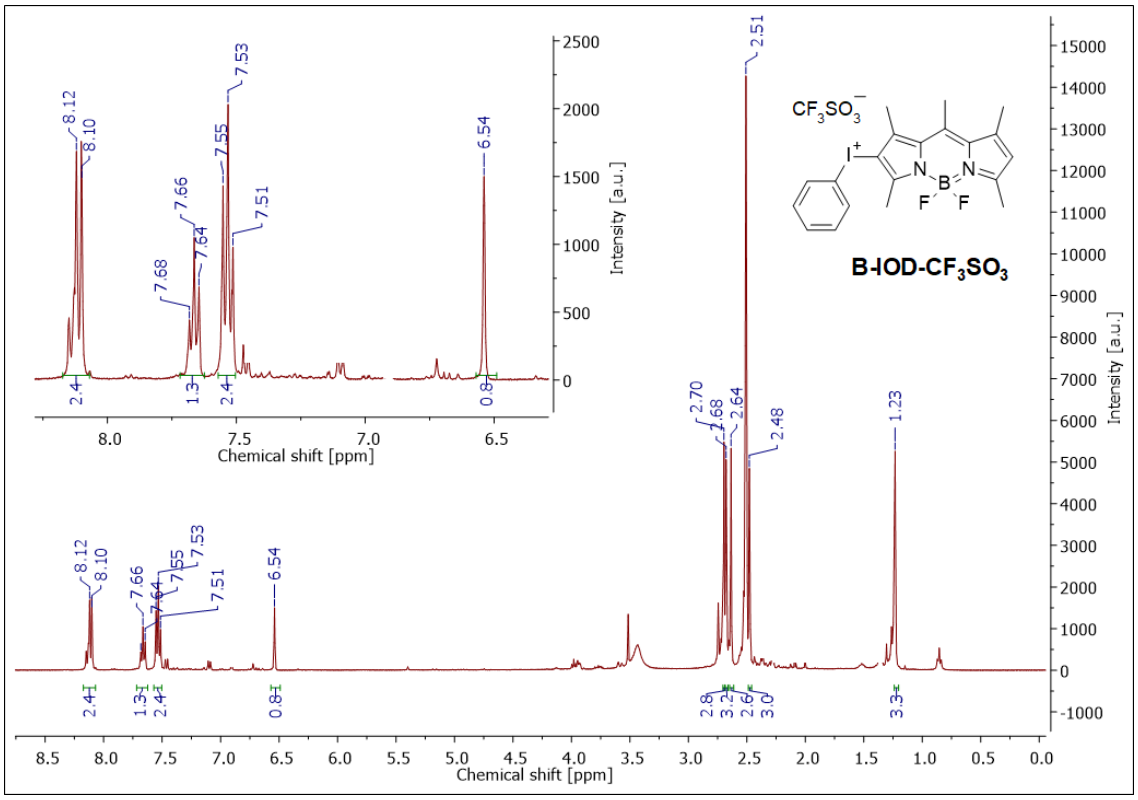

Figure S7. ^{1}H NMR spectrum of hexafluorophosphate phenyl[4,4-difluoro-1,3,5,7,8-pentametylo-4-bora-3a, 4a-diaza-s -indacene]iodonium.

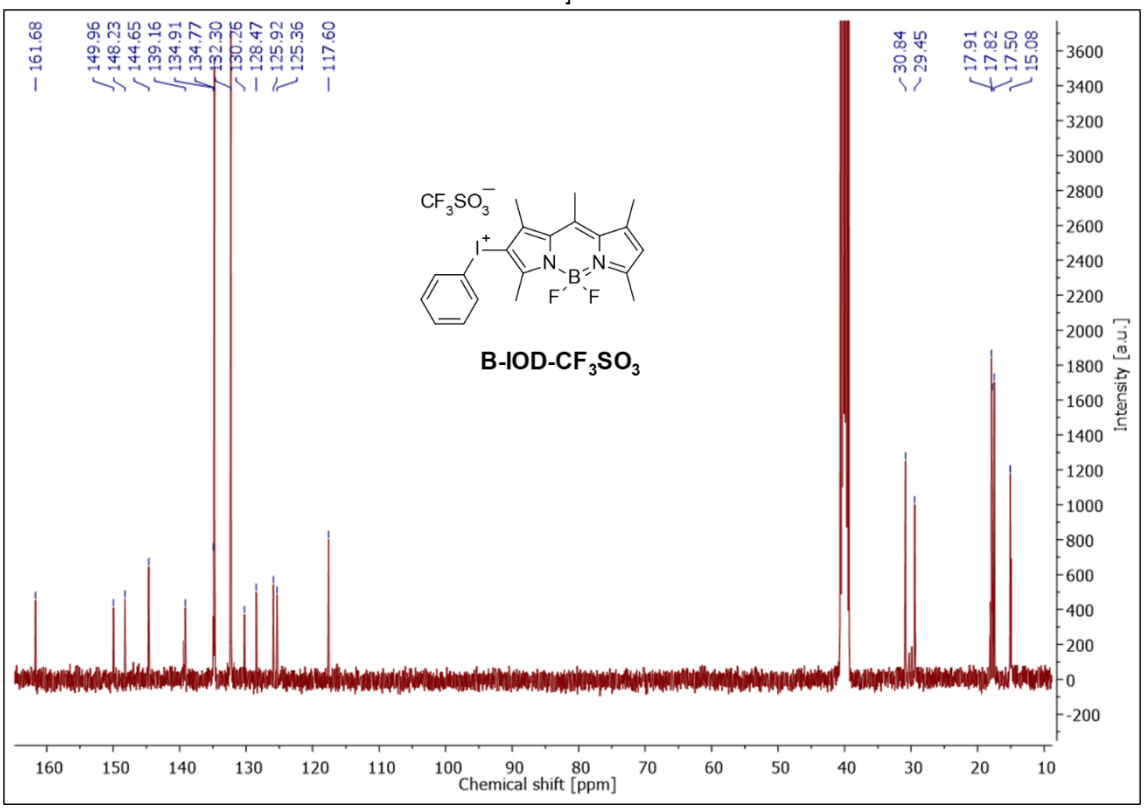

Figure S8. ^{13}C NMR spectrum of hexafluorophosphate phenyl[4,4-difluoro-1,3,5,7,8-pentametylo-4-bora-3a, 4a-diaza-s -indacene]iodonium.

Cyclic voltammetry curves showing reduction processes of iodonium salts in acetonitrile

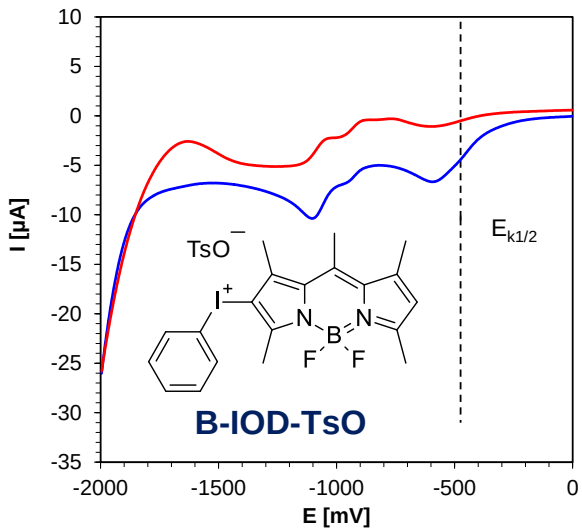

Figure S9: Cyclic voltammogram curves of the B-IOD-TsO reduction in acetonitrile.

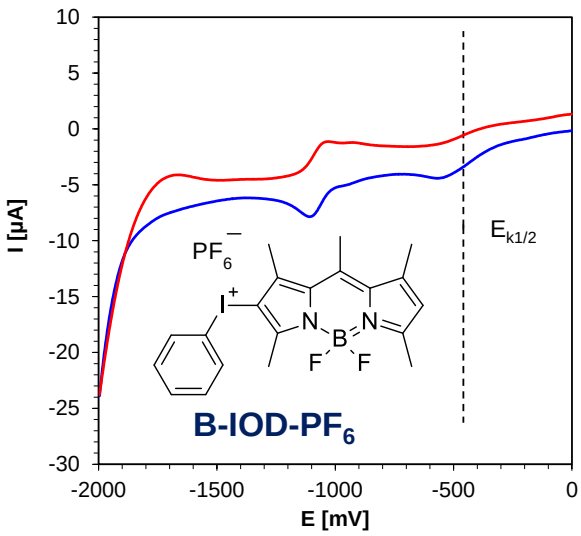

Figure S10: Cyclic voltammogram curves of the B-IOD-PF_6 reduction in acetonitrile.

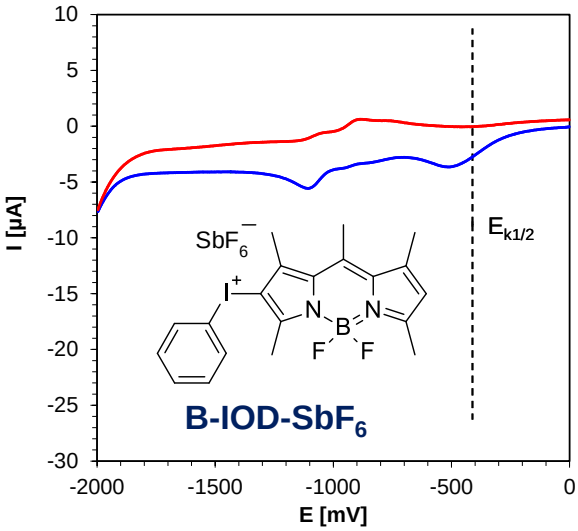

Figure S11: Cyclic voltammogram curves of the B-IOD-SbF_6 reduction in acetonitrile.

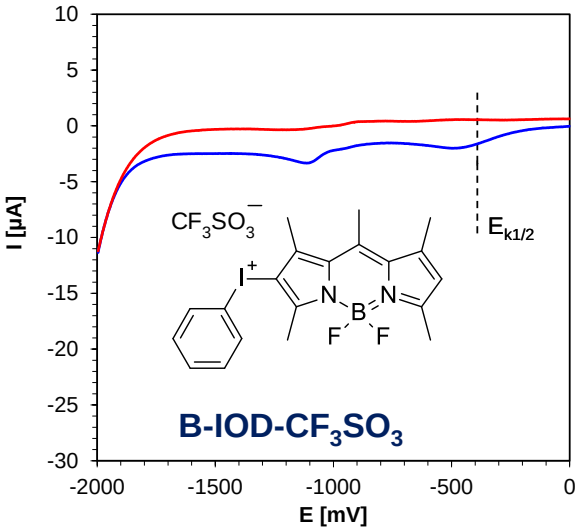

Figure S12: Cyclic voltammogram curves of the B-IOD-CF_3SO_3 reduction in acetonitrile.

The optimized structures and HOMO and LUMO orbitals of investigated iodonium salts free molecules determined with the use of uB3LYP/6-31G* level of theory

Compound	HOMO	LUMO
B-1 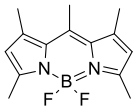 *4,4-difluoro-1,3,5,7,8-pentamethyl-4-bora-3a,4a-diaza-s-indecene*	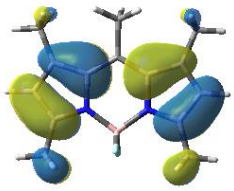	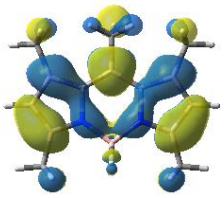
CATION 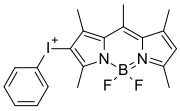 *phenyl[4,4-difluoro-1,3,5,7,8-pentametylo-4-bora-3a, 4a-diaza-s-indacene]iodonium*	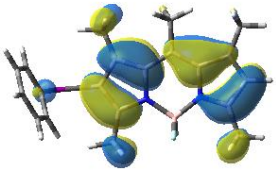	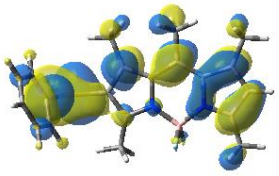

Steady state photolysis upon exposure with LED @470 nm of investigated new iodonium salts in acetonitrile

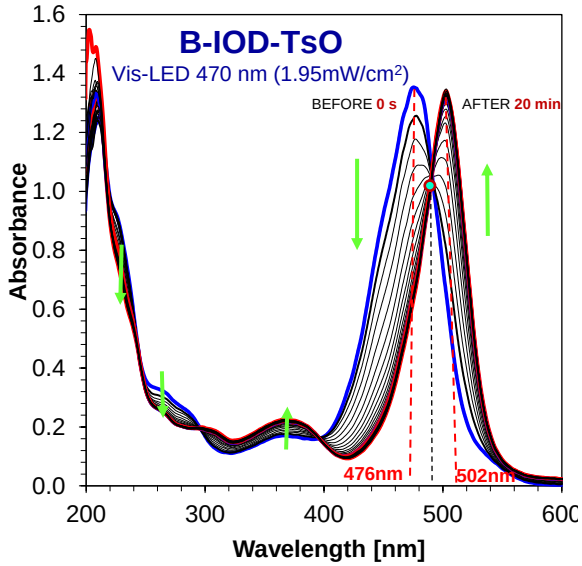

Figure S13: Steady state photolysis of B-IOD-TsO under irradiation upon Vis-LED at 470 nm (1.95 mW/cm^2).

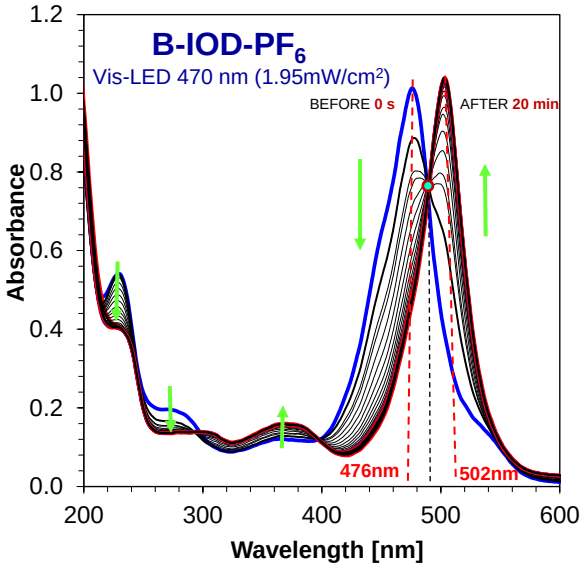

Figure S14: Steady state photolysis of B-IOD-PF_6 under irradiation upon Vis-LED at 470 nm (1.95 mW/cm^2).

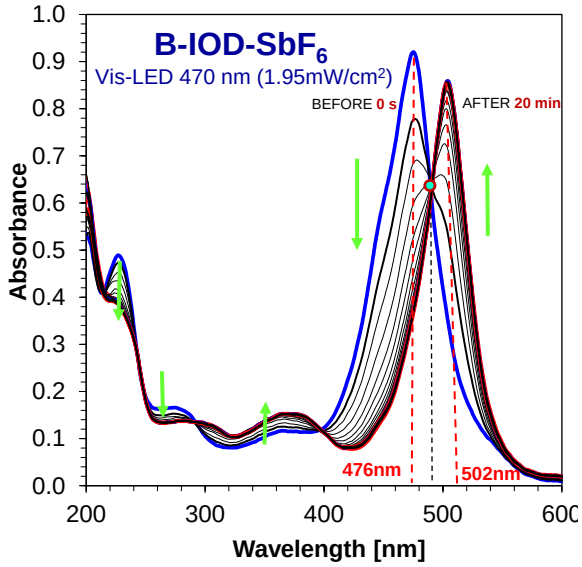

Figure S15: Steady state photolysis of B-IOD-SbF_6 under irradiation upon Vis-LED at 470 nm (1.95 mW/cm^2).

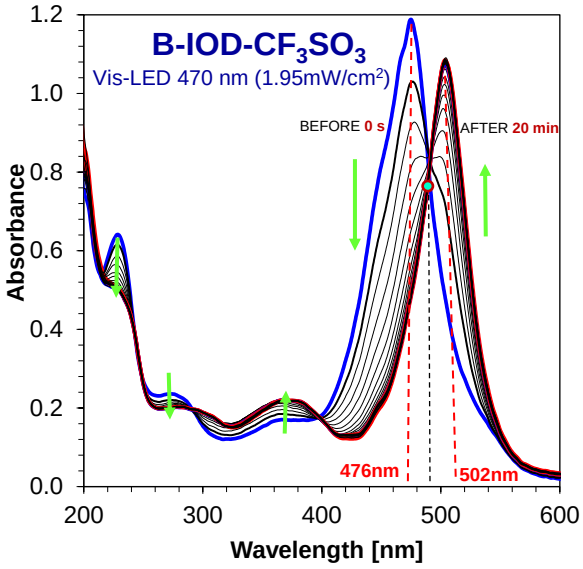

Figure S16: Steady state photolysis of B-IOD-CF_3SO_3 under irradiation upon Vis-LED at 470 nm (1.95 mW/cm^2).

Steady state photolysis of investigated new iodonium salts in acetonitrile upon exposure with visible LED @470 nm with different irradiation

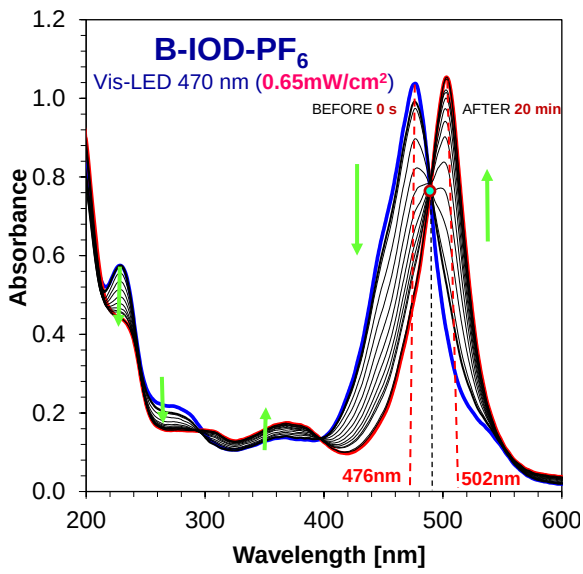

Figure S17: Steady state photolysis of hexafluorophosphate phenyl[4,4-difluoro-1,3,5,7,8-pentametylo-4-bora-3a, 4a-diaza-s-indacene]iodonium under irradiation upon Vis-LED at 470 nm (0.65 mW/cm^2).

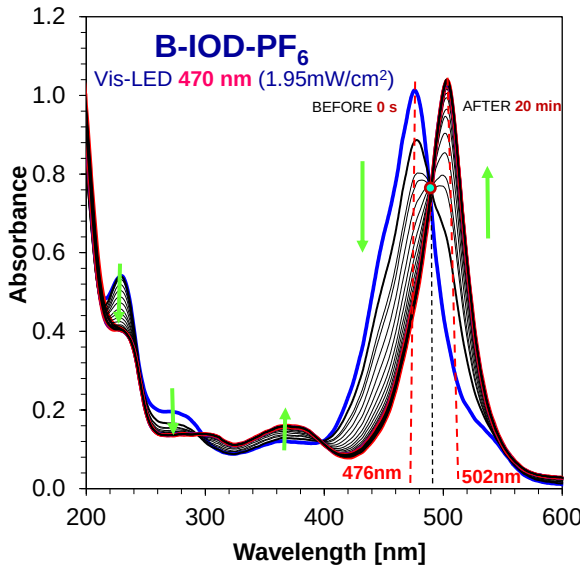

Figure S18: Steady state photolysis of hexafluorophosphate phenyl[4,4-difluoro-1,3,5,7,8-pentametylo-4-bora-3a, 4a-diaza-s-indacene]iodonium under irradiation upon Vis-LED at 470 nm (1.95 mW/cm^2).

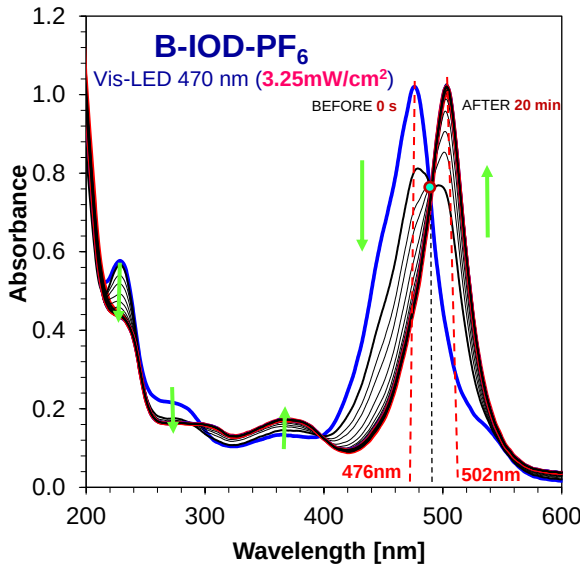

Figure S19: Steady state photolysis of hexafluorophosphate phenyl[4,4-difluoro-1,3,5,7,8-pentametylo-4-bora-3a, 4a-diaza-s-indacene]iodonium under irradiation upon Vis-LED at 470 nm (3.25 mW/cm^2).

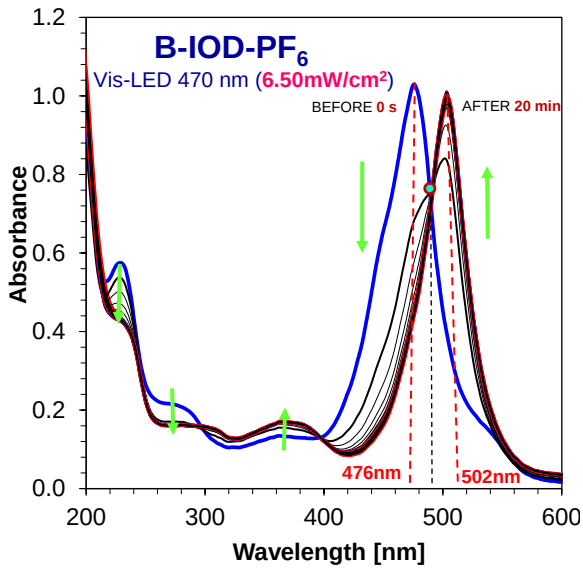

Figure S20: Steady state photolysis of hexafluorophosphate phenyl[4,4-difluoro-1,3,5,7,8-pentametylo-4-bora-3a, 4a-diaza-s-indacene]iodonium under irradiation upon Vis-LED at 470 nm (6.50 mW/cm^2).

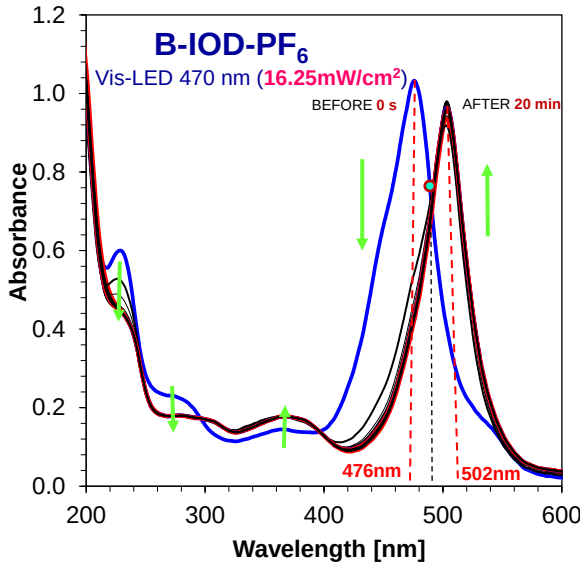

Figure S21: Steady state photolysis of hexafluorophosphate phenyl[4,4-difluoro-1,3,5,7,8-pentametylo-4-bora-3a, 4a-diaza-s-indacene]iodonium under irradiation upon Vis-LED at 470 nm (16.25 mW/cm^2).

Steady state photolysis upon exposure with UV-LED and visible LED of investigated new iodonium salts in acetonitrile

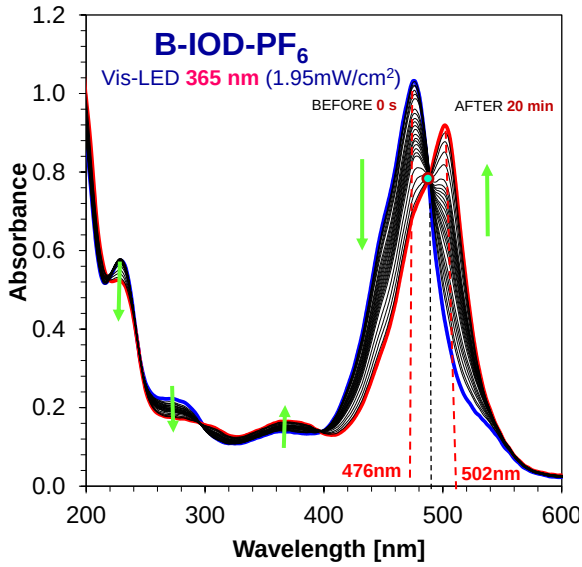

Figure S22: Steady state photolysis of hexafluorophosphate phenyl[4,4-difluoro-1,3,5,7,8-pentametylo-4-bora-3a, 4a-diaza-s-indacene]iodonium under irradiation upon UV-LED at 365 nm (1.95 mW/cm^2).

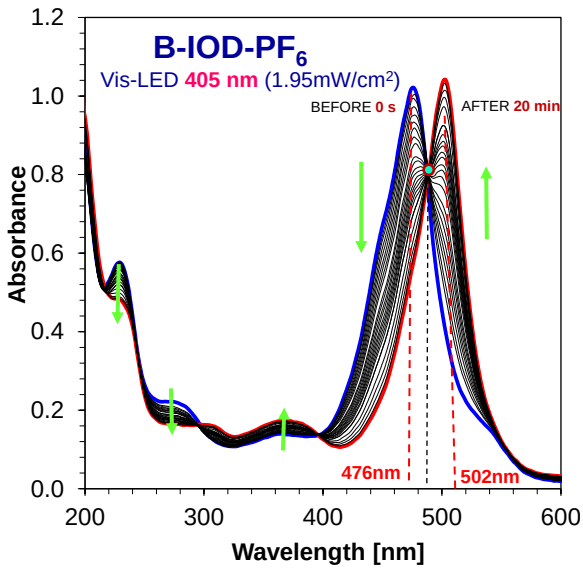

Figure S23: Steady state photolysis of hexafluorophosphate phenyl[4,4-difluoro-1,3,5,7,8-pentametylo-4-bora-3a, 4a-diaza-s-indacene]iodonium under irradiation upon Vis-LED at 405 nm (1.95 mW/cm^2).

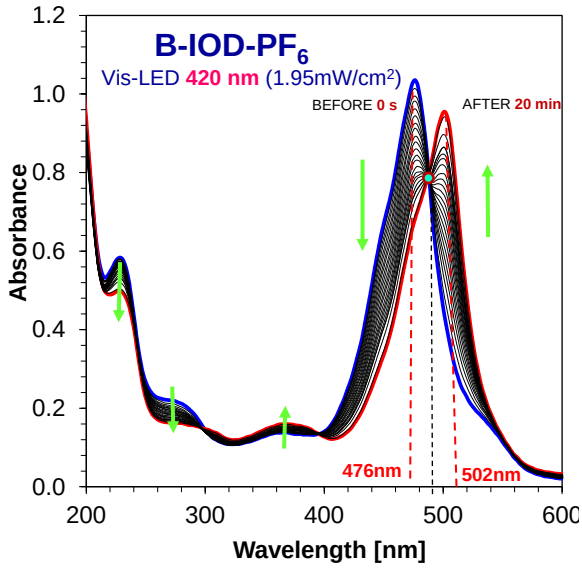

Figure S24: Steady state photolysis of hexafluorophosphate phenyl[4,4-difluoro-1,3,5,7,8-pentametylo-4-bora-3a, 4a-diaza-s-indacene]iodonium under irradiation upon Vis-LED at 420 nm (1.95 mW/cm^2).

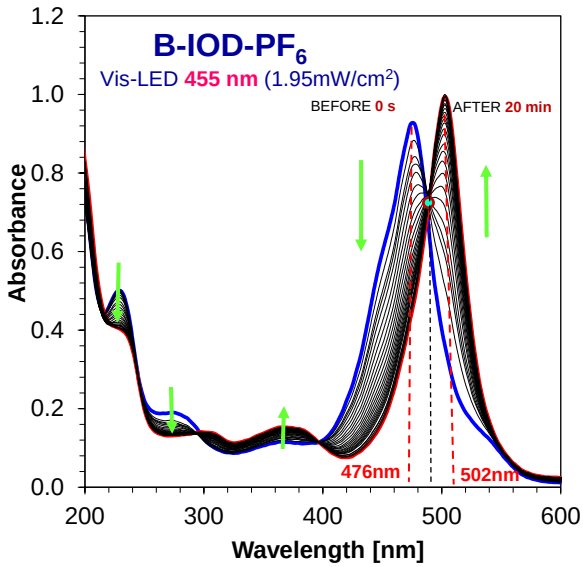

Figure S25: Steady state photolysis of hexafluorophosphate phenyl[4,4-difluoro-1,3,5,7,8-pentametylo-4-bora-3a, 4a-diaza-s-indacene]iodonium under irradiation upon Vis-LED at 455 nm (1.95 mW/cm^2).

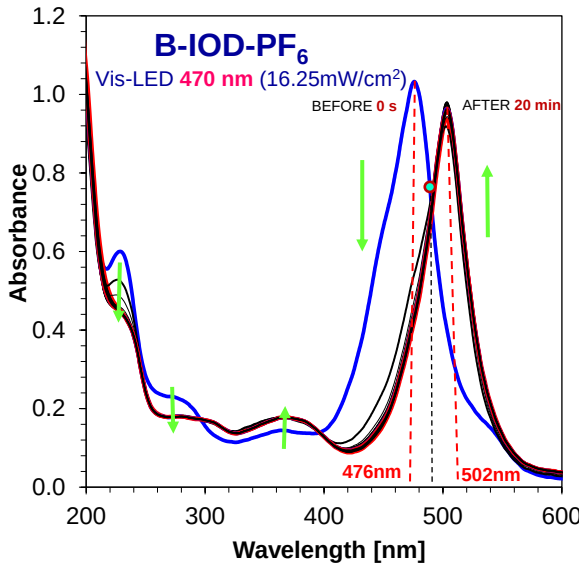

Figure S26: Steady state photolysis of hexafluorophosphate phenyl[4,4-difluoro-1,3,5,7,8-pentametylo-4-bora-3a, 4a-diaza-s-indacene]iodonium under irradiation upon Vis-LED at 470 nm (1.95 mW/cm^2).

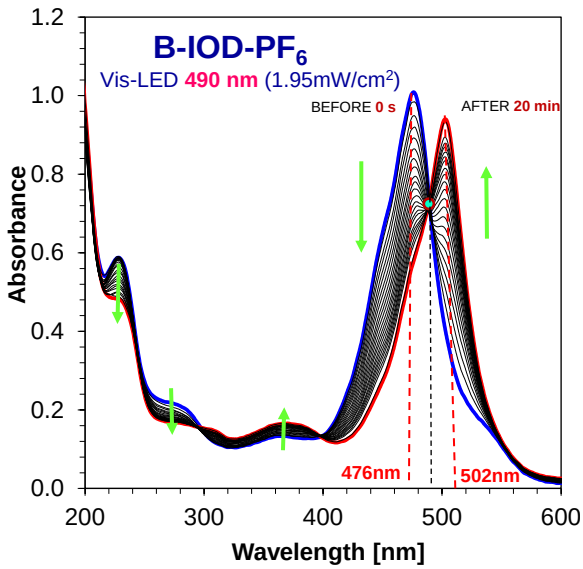

Figure S27: Steady state photolysis of hexafluorophosphate phenyl[4,4-difluoro-1,3,5,7,8-pentametylo-4-bora-3a, 4a-diaza-s-indacene]iodonium under irradiation upon Vis-LED at 490 nm (1.95 mW/cm^2).

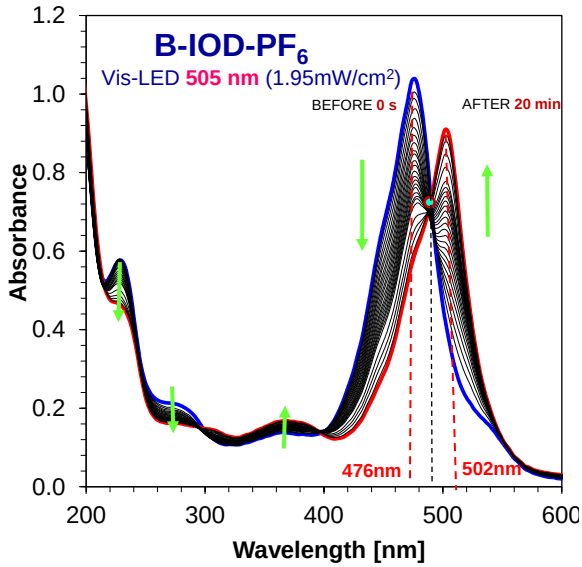

Figure S28: Steady state photolysis of hexafluorophosphate phenyl[4,4-difluoro-1,3,5,7,8-pentametylo-4-bora-3a, 4a-diaza-s-indacene]iodonium under irradiation upon Vis-LED at 505nm (1.95 mW/cm^2).

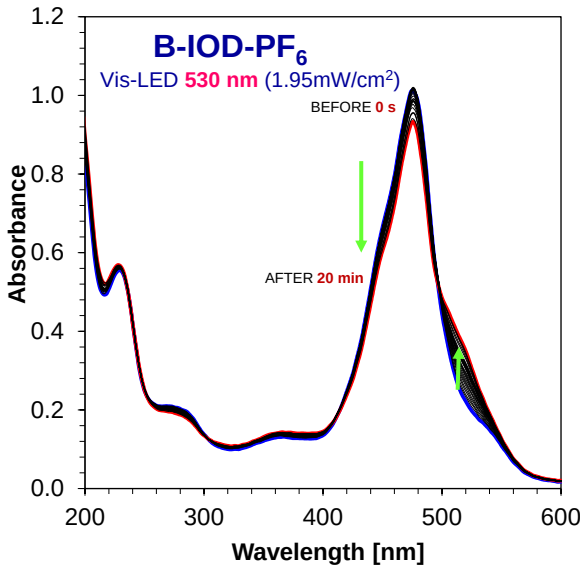

Figure S29: Steady state photolysis of hexafluorophosphate phenyl[4,4-difluoro-1,3,5,7,8-pentametylo-4-bora-3a, 4a-diaza-s-indacene]iodonium under irradiation upon Vis-LED at 530 nm (1.95 mW/cm^2).

Applicability of BODIPY derivatives for on-line monitoring progress of ring opening photopolymerization of epoxy CADE monomer under visible LED 470 nm and different amount of initiators

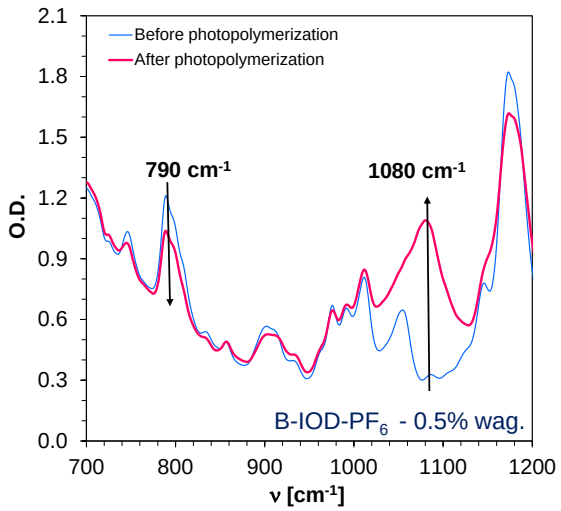

Fig. S30: FT-IR spectra before and after photopolymerization of CADE monomer under Vis-LED 470 nm irradiation (12.7 mW/cm^2) in composition with B-IOD-PF_6 (0.5% wag.) compound as the photoinitiator.

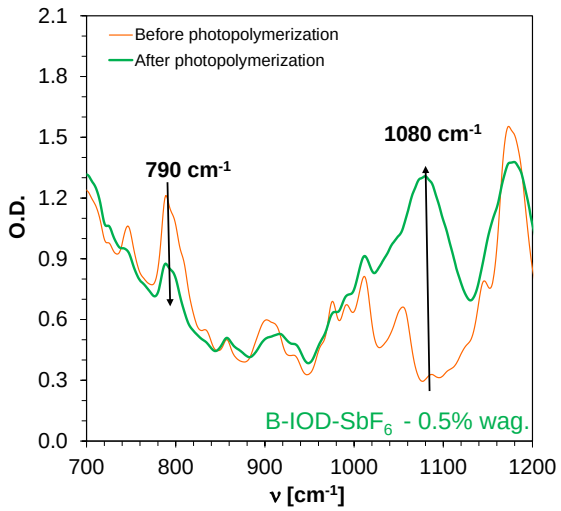

Fig. S31: FT-IR spectra before and after photopolymerization of CADE monomer under Vis-LED 470 nm irradiation (12.7 mW/cm^2) in composition with B-IOD-SbF_6 (0.5% wag.) compound as the photoinitiator.

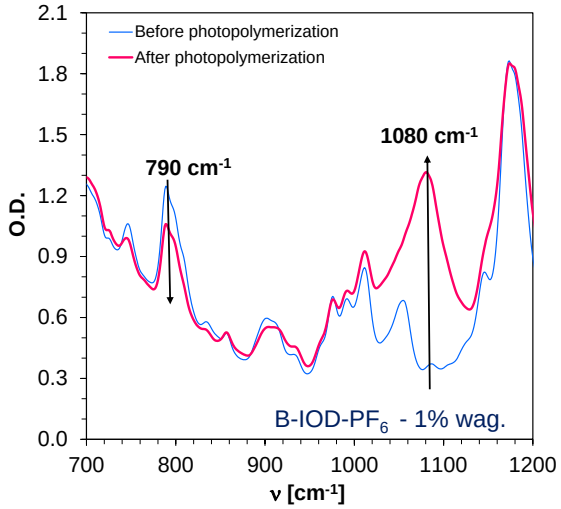

Fig. S32: FT-IR spectra before and after photopolymerization of CADE monomer under Vis-LED 470 nm irradiation (12.7 mW/cm^2) in composition with B-IOD-PF_6 (1% wag.) compound as the photoinitiator.

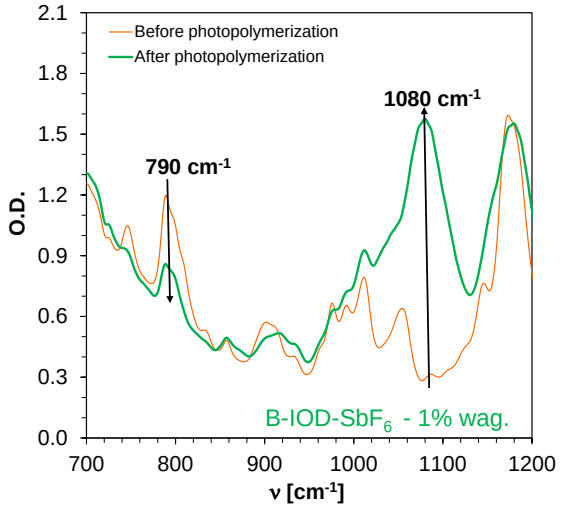

Fig. S33: FT-IR spectra before and after photopolymerization of CADE monomer under Vis-LED 470 nm irradiation (12.7 mW/cm^2) in composition with B-IOD-SbF_6 (1% wag.) compound as the photoinitiator.

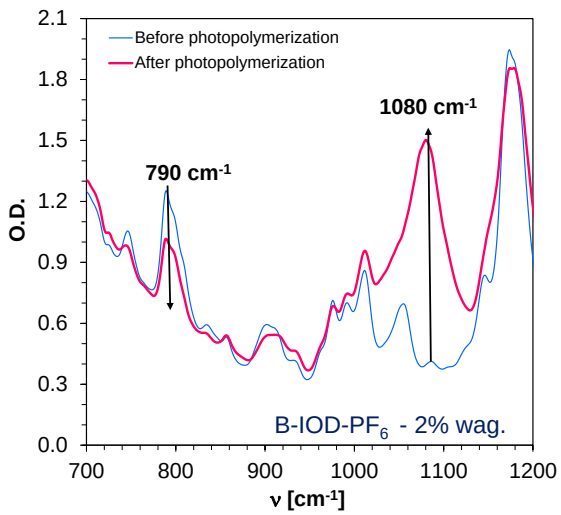

Fig. S34: FT-IR spectra before and after photopolymerization of CADE monomer under Vis-LED 470 nm irradiation (12.7 mW/cm^2) in composition with B-IOD-PF_6 (2% wag.) compound as the photoinitiator.

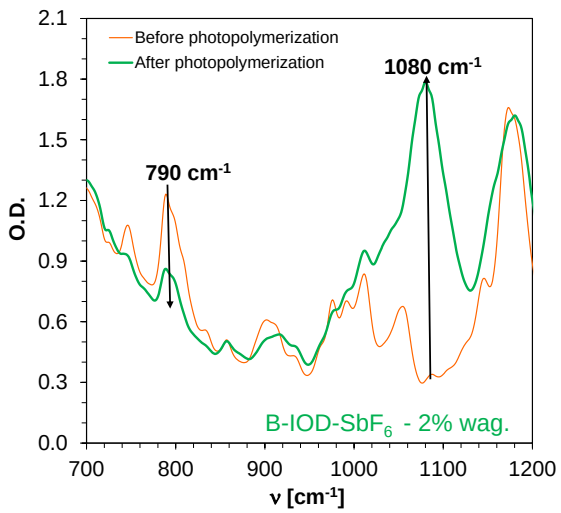

Fig. S35: FT-IR spectra before and after photopolymerization of CADE monomer under Vis-LED 470 nm irradiation (12.7 mW/cm^2) in composition with B-IOD-SbF_6 (2% wag.) compound as the photoinitiator.

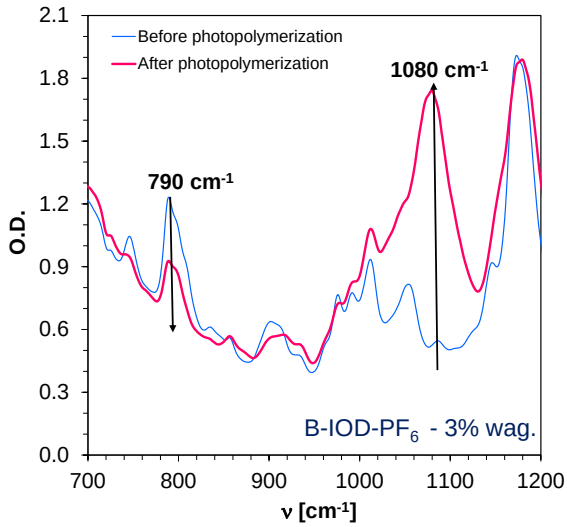

Fig. S36: FT-IR spectra before and after photopolymerization of CADE monomer under Vis-LED 470 nm irradiation (12.7 mW/cm^2) in composition with B-IOD-PF_6 (3% wag.) compound as the photoinitiator.

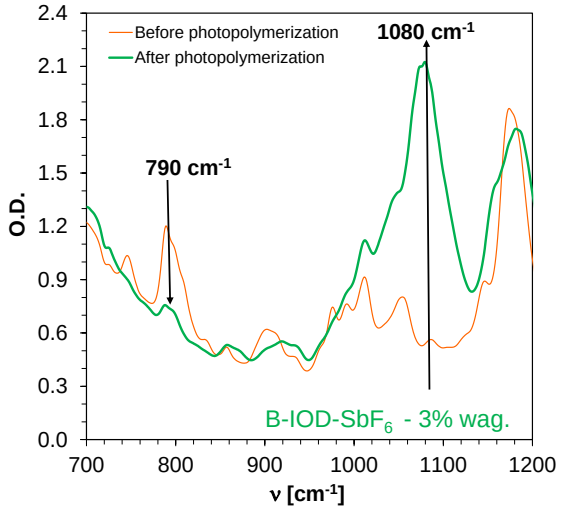

Fig. S37: FT-IR spectra before and after photopolymerization of CADE monomer under Vis-LED 470 nm irradiation (12.7 mW/cm^2) in composition with B-IOD-SbF_6 (3% wag.) compound as the photoinitiator.

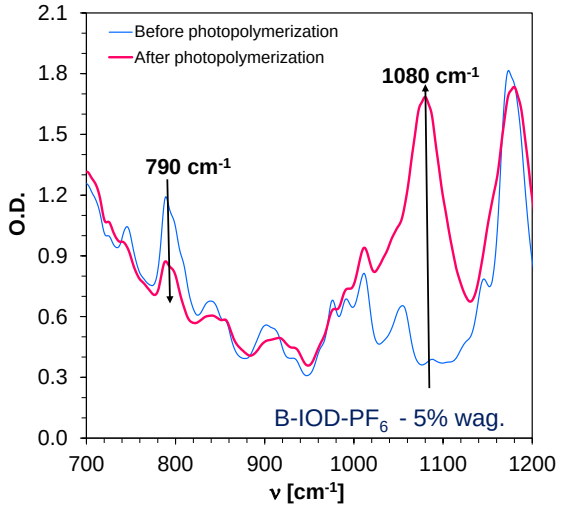

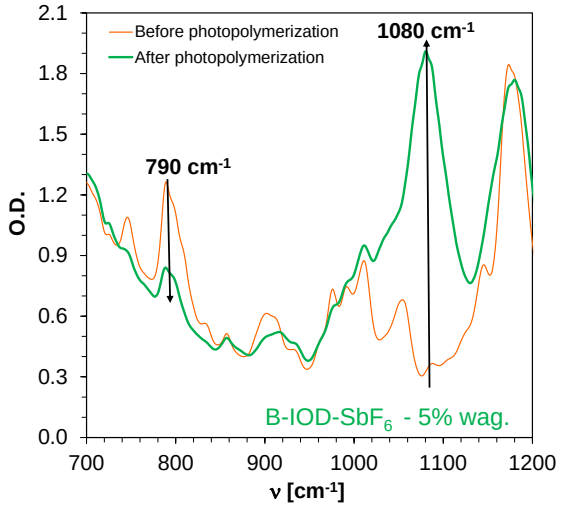

Fig. S38: FT-IR spectra before and after photopolymerization of CADE monomer under Vis-LED 470 nm irradiation (12.7 mW/cm^2) in composition with B-IOD-PF$_6$ (5% wag.) compound as the photoinitiator.

Fig. S39: FT-IR spectra before and after photopolymerization of CADE monomer under Vis-LED 470 nm irradiation (12.7 mW/cm^2) in composition with B-IOD-SbF$_6$ (5% wag.) compound as the photoinitiator.

Applicability of B-IOD-PF$_6$ for on-line monitoring progress of ring opening photopolymerization of epoxy CADE monomer under different diodes

Different diodes and the same intensity on the sample 22.8 mW/cm^2

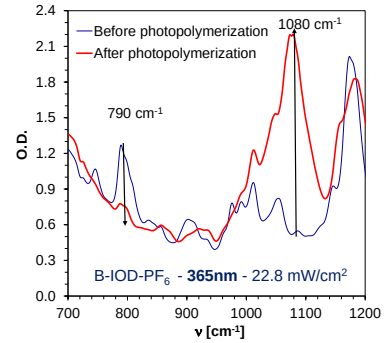

Fig. S40: FT-IR spectra before and after photopolymerization of CADE monomer under UV-LED 365 nm irradiation (22.8 mW/cm^2) in composition with B-IOD-PF$_6$ (3% wag.) compound as the photoinitiator.

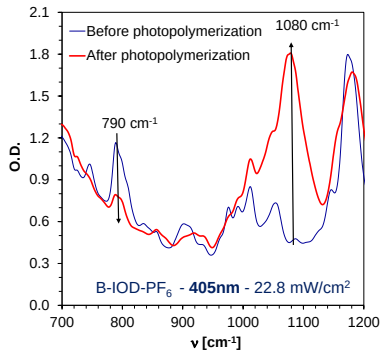

Fig. S41: FT-IR spectra before and after photopolymerization of CADE monomer under Vis-LED 405 nm irradiation (22.8 mW/cm^2) in composition with B-IOD-PF$_6$ (3% wag.) compound as the photoinitiator.

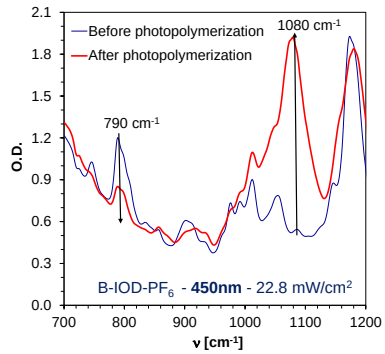

Fig. S42: FT-IR spectra before and after photopolymerization of CADE monomer under Vis-LED 450 nm irradiation (22.8 mW/cm^2) in composition with B-IOD-PF$_6$ (3% wag.) compound as the photoinitiator.

Different diodes and the maximum intensity of sample

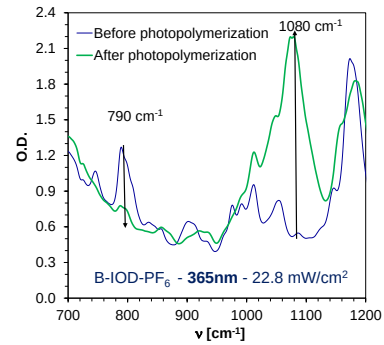

Fig. S43: FT-IR spectra before and after photopolymerization of CADE monomer under UV-LED 365 nm irradiation (22.8 mW/cm^2) in composition with B-IOD-PF$_6$ (3% wag.) compound as the photoinitiator.

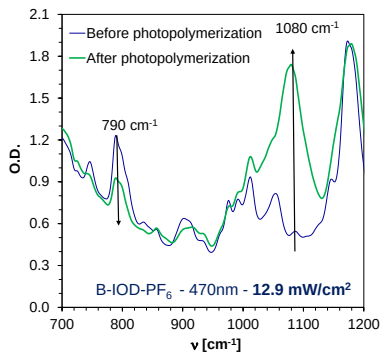

Fig. S44: FT-IR spectra before and after photopolymerization of CADE monomer under Vis-LED 470 nm irradiation (12.9 mW/cm^2) in composition with B-IOD-PF$_6$ (3% wag.) compound as the photoinitiator.

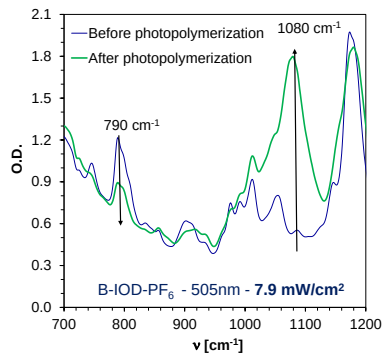

Fig. S45: FT-IR spectra before and after photopolymerization of CADE monomer under Vis-LED 505 nm irradiation (7.9 mW/cm^2) in composition with B-IOD-PF$_6$ (3% wag.) compound as the photoinitiator.

Dark polymerization: Applicability of B-IOD-PF$_6$ for on-line monitoring progress of ring opening photopolymerization of epoxy CADE monomer under different diodes. The light switched after 350s

Different diodes and the same intensity of sample 22.8 mW/cm^2

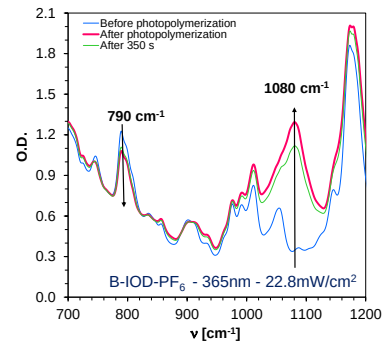

Fig. S46: FT-IR spectra before and after photopolymerization of CADE monomer under UV-LED 365 nm irradiation (22.8 mW/cm^2) in composition with B-IOD-PF$_6$ (3% wag.) compound as the photoinitiator. The light switched after 350s.

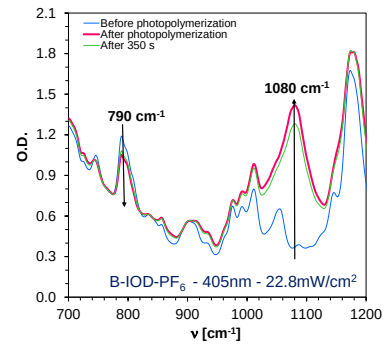

Fig. S47: FT-IR spectra before and after photopolymerization of CADE monomer under Vis-LED 405 nm irradiation (22.8 mW/cm^2) in composition with B-IOD-PF$_6$ (3% wag.) compound as the photoinitiator. The light switched after 350s.

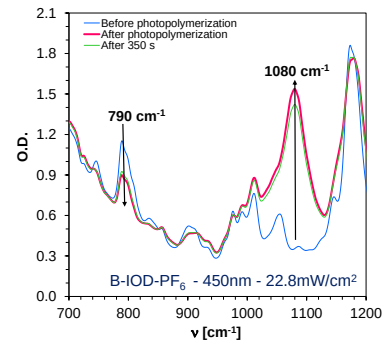

Fig. S48: FT-IR spectra before and after photopolymerization of CADE monomer under Vis-LED 450 nm irradiation (22.8 mW/cm^2) in composition with B-IOD-PF$_6$ (3% wag.) compound as the photoinitiator. The light switched after 350s.

Different diodes and the maximum intensity of sample

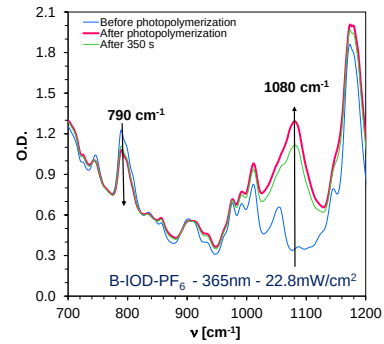

Fig. S49: FT-IR spectra before and after photopolymerization of CADE monomer under UV-LED 365 nm irradiation (22.8 mW/cm^2) in composition with B-IOD-PF$_6$ (3% wag.) compound as the photoinitiator. The light switched after 350s.

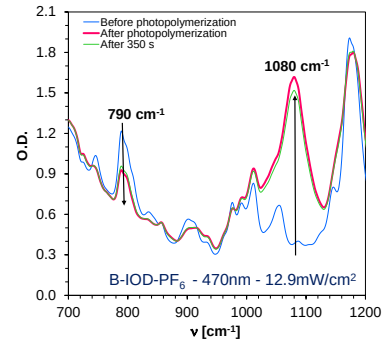

Fig. S50: FT-IR spectra before and after photopolymerization of CADE monomer under Vis-LED 470 nm irradiation (12.9 mW/cm^2) in composition with B-IOD-PF$_6$ (3% wag.) compound as the photoinitiator. The light switched after 350s.

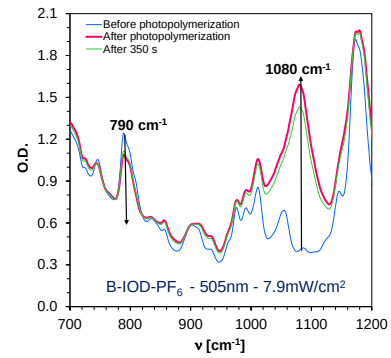

Fig. S51: FT-IR spectra before and after photopolymerization of CADE monomer under Vis-LED 505 nm irradiation (7.9 mW/cm^2) in composition with B-IOD-PF$_6$ (3% wag.) compound as the photoinitiator. The light switched after 350s.

Dark polymerization: Applicability of B-IOD-PF$_6$ for on-line monitoring progress of ring opening photopolymerization of epoxy CADE monomer under Vis-LED 505nm (7.9mW/cm^2). The light switched after different time

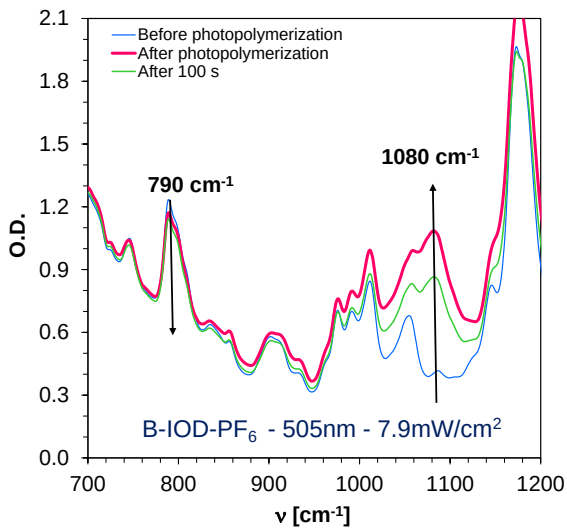

Fig. S52: FT-IR spectra before and after photopolymerization of CADE monomer under Vis-LED 505 nm irradiation (7.9 mW/cm^2) in composition with B-IOD-PF$_6$ (3% wag.) compound as the photoinitiator. The light switched after 100s.

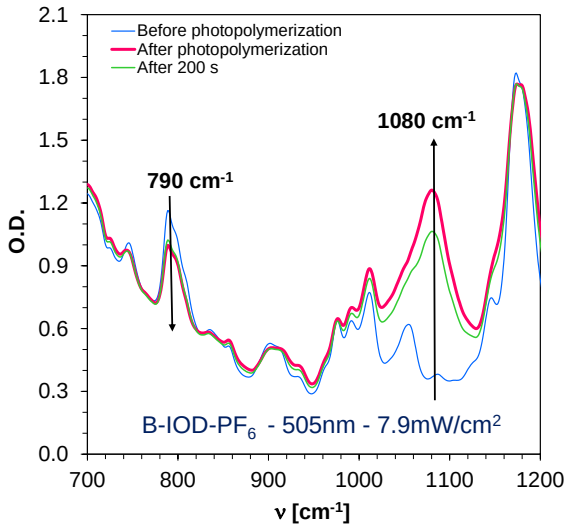

Fig. S53: FT-IR spectra before and after photopolymerization of CADE monomer under Vis-LED 505 nm irradiation (7.9 mW/cm^2) in composition with B-IOD-PF$_6$ (3% wag.) compound as the photoinitiator. The light switched after 200s.

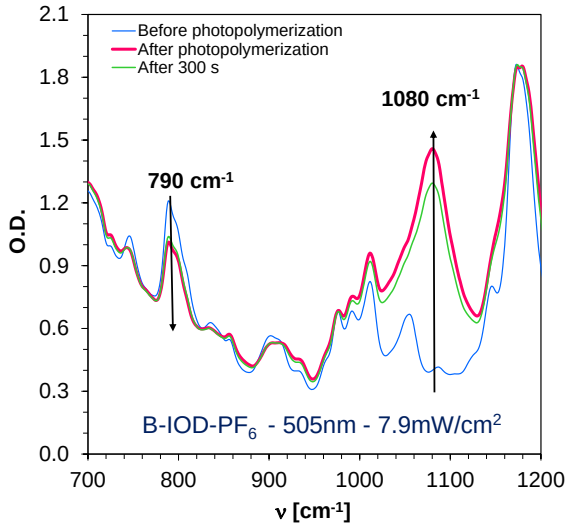

Fig. S54: FT-IR spectra before and after photopolymerization of CADE monomer under Vis-LED 505 nm irradiation (7.9 mW/cm^2) in composition with B-IOD-PF$_6$ (3% wag.) compound as the photoinitiator. The light switched after 300s.

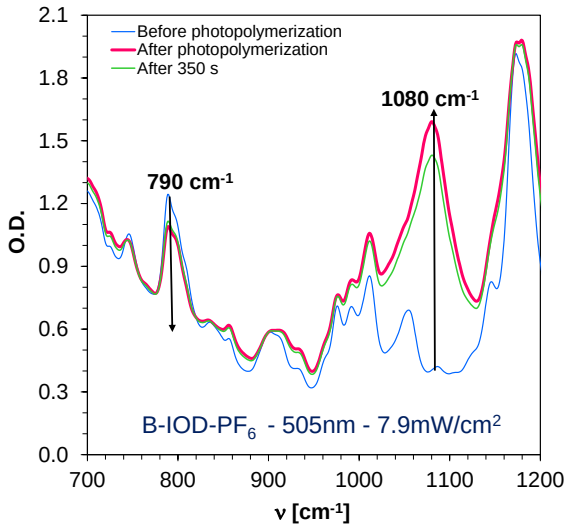

Fig. S55: FT-IR spectra before and after photopolymerization of CADE monomer under Vis-LED 505 nm irradiation (7.9 mW/cm^2) in composition with B-IOD-PF$_6$ (3% wag.) compound as the photoinitiator. The light switched after 350s.

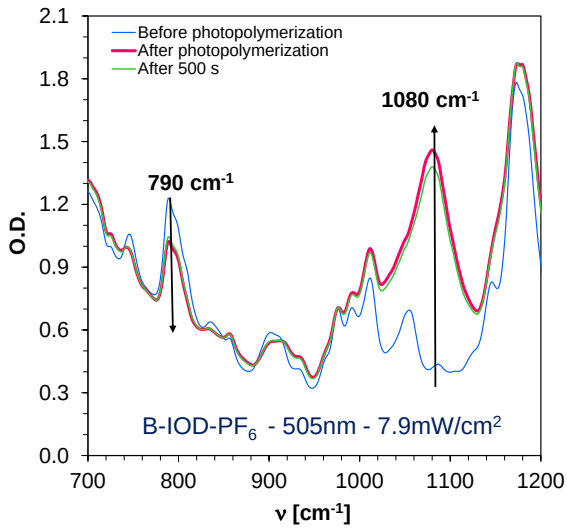

Fig. S56: FT-IR spectra before and after photopolymerization of CADE monomer under Vis-LED 505 nm irradiation (7.9 mW/cm^2) in composition with B-IOD-PF$_6$ (3% wag.) compound as the photoinitiator. The light switched after 500s.

Applicability of B-IOD-PF$_6$ for on-line monitoring progress of photopolymerization of vinyl TEGDVE monomer under different diodes

Different diodes and the same intensity of sample 12.9 mW/cm^2

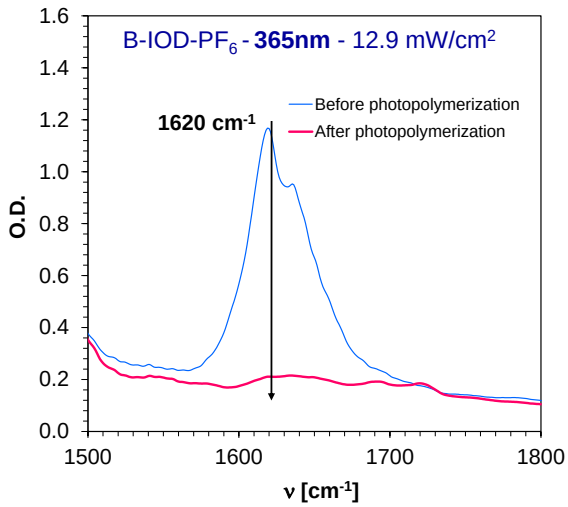

Fig. S57: FT-IR spectra before and after photopolymerization of TEGDVE monomer under UV-LED 365 nm irradiation (12.9 mW/cm^2) in composition with B-IOD-PF$_6$ (3% wag.) compound as the photoinitiator.

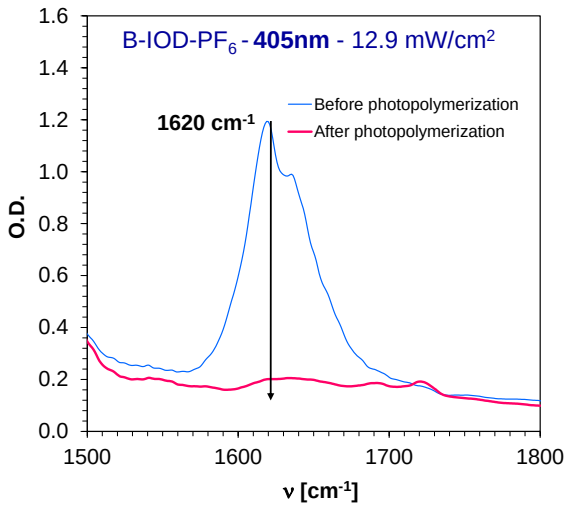

Fig. S58: FT-IR spectra before and after photopolymerization of TEGDVE monomer under Vis-LED 405 nm irradiation (12.9 mW/cm^2) in composition with B-IOD-PF$_6$ (3% wag.) compound as the photoinitiator.

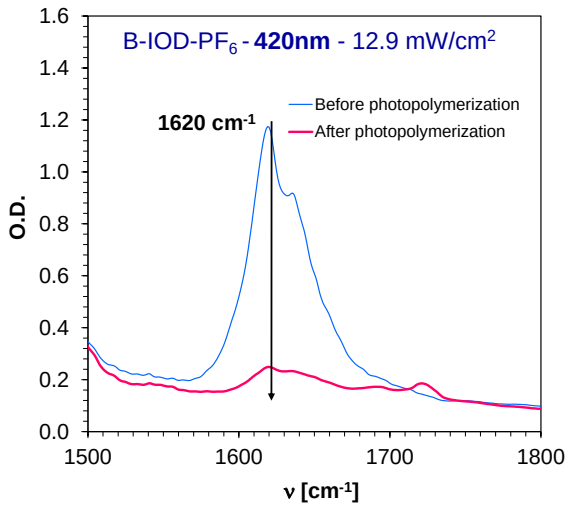

Fig. S59: FT-IR spectra before and after photopolymerization of TEGDVE monomer under Vis-LED 420 nm irradiation (12.9 mW/cm^2) in composition with B-IOD-PF$_6$ (3% wag.) compound as the photoinitiator.

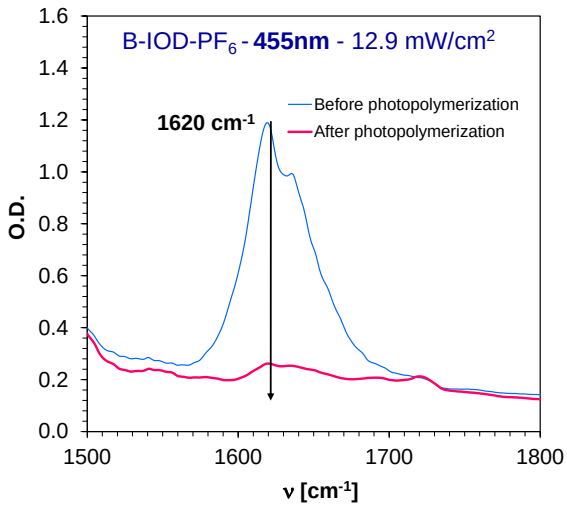

Fig. S60: FT-IR spectra before and after photopolymerization of TEGDVE monomer under Vis-LED 455 nm irradiation (12.9 mW/cm^2) in composition with B-IOD-PF$_6$ (3% wag.) compound as the photoinitiator.

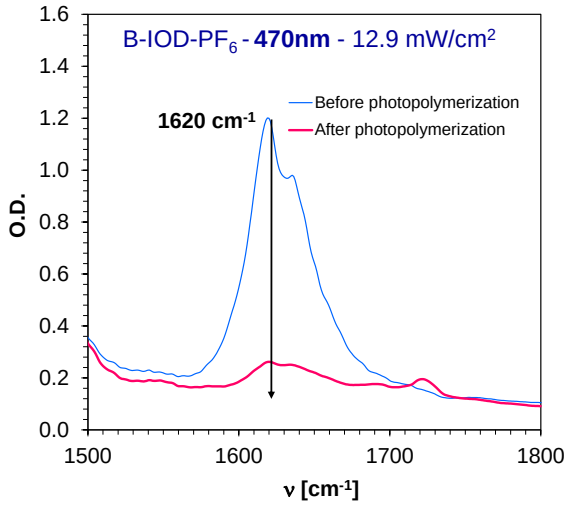

⇐ **Fig. S61:** FT-IR spectra before and after photopolymerization of TEGDVE monomer under Vis-LED 470 nm irradiation (12.9 mW/cm^2) in composition with B-IOD-PF$_6$ (3% wag.) compound as the photoinitiator.

Different diodes and the maximum intensity of sample

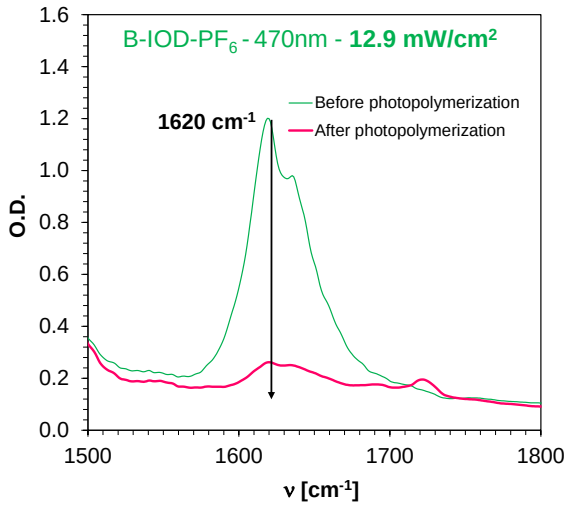

Fig. S62: FT-IR spectra before and after photopolymerization of TEGDVE monomer under Vis-LED

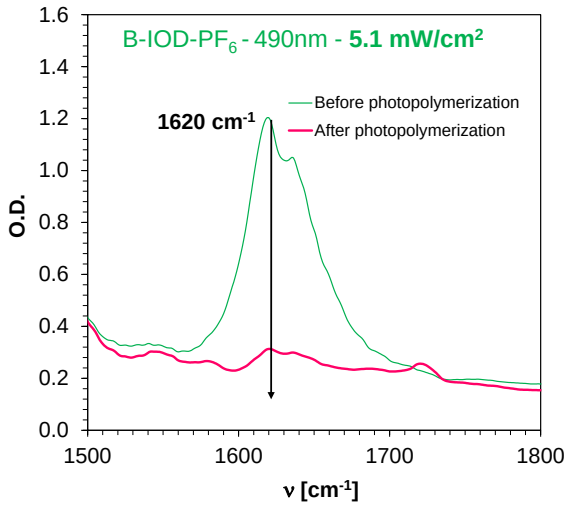

Fig. S63: FT-IR spectra before and after photopolymerization of TEGDVE monomer under Vis-LED

470 nm irradiation (12.9 mW/cm^2) in composition with B-IOD-PF$_6$ (3% wag.) compound as the photoinitiator.

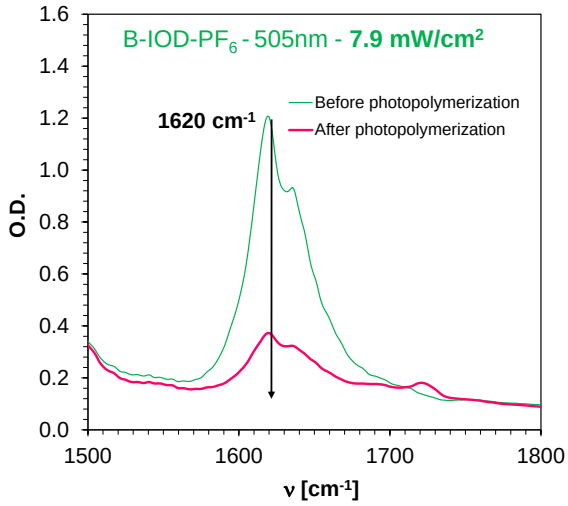

Fig. S64: FT-IR spectra before and after photopolymerization of TEGDVE monomer under Vis-LED 505 nm irradiation (7.9 mW/cm^2) in composition with B-IOD-PF$_6$ (3% wag.) compound as the photoinitiator.

490 nm irradiation (5.1 mW/cm^2) in composition with B-IOD-PF$_6$ (3% wag.) compound as the photoinitiator.

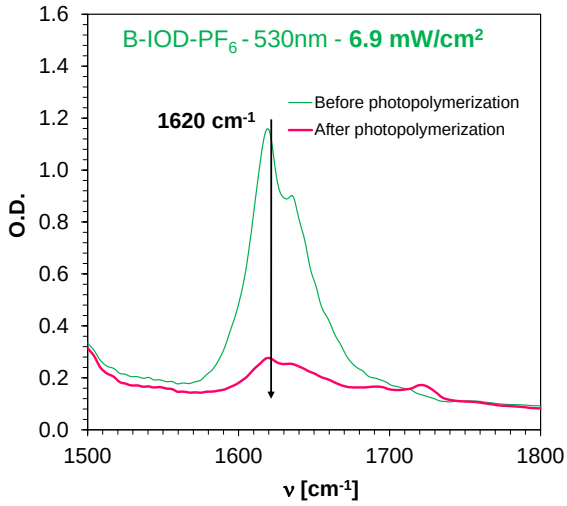

Fig. S65: FT-IR spectra before and after photopolymerization of TEGDVE monomer under Vis-LED 530 nm irradiation (6.9 mW/cm^2) in composition with B-IOD-PF$_6$ (3% wag.) compound as the photoinitiator.

Applicability of BODIPY derivatives for on-line monitoring progress of ring opening photopolymerization of epoxy CADE monomer under visible LED 470 nm (12.9 mW/cm^2)

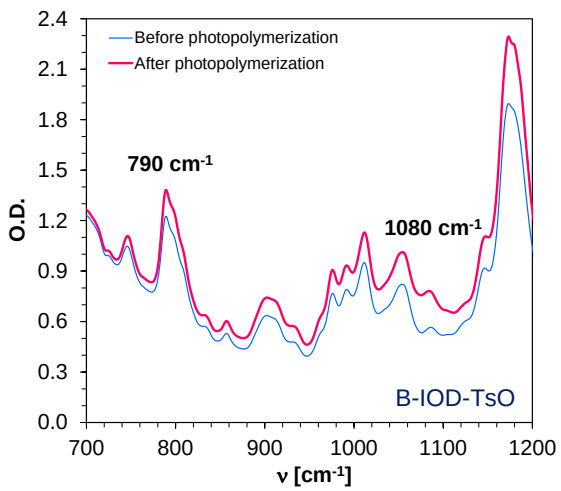

Fig. S66: FT-IR spectra before and after photopolymerization of CADE monomer under Vis-LED 470 nm irradiation (12.9 mW/cm^2) in composition with B-IOD-TsO (3% wag.) compound as the photoinitiator.

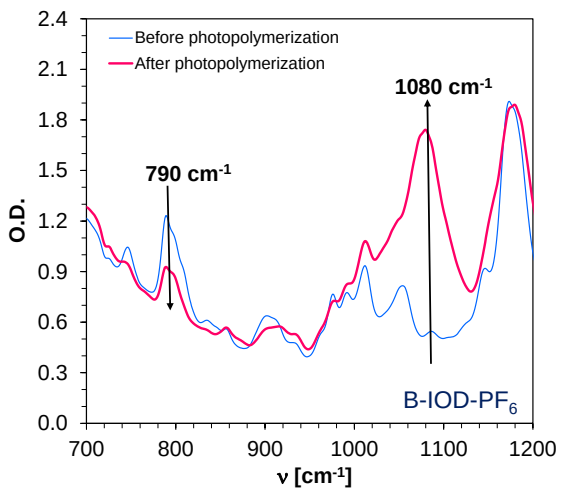

Fig. S67: FT-IR spectra before and after photopolymerization of CADE monomer under Vis-LED 470 nm irradiation (12.9 mW/cm^2) in composition with B-IOD-PF$_6$ (3% wag.) compound as the photoinitiator.

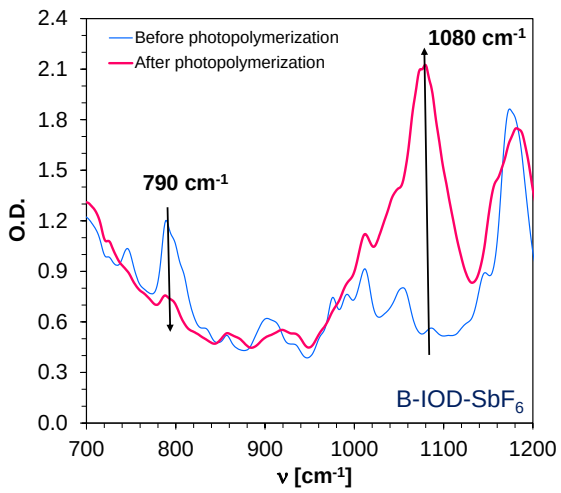

Fig. S68: FT-IR spectra before and after photopolymerization of CADE monomer under Vis-LED 470 nm irradiation (12.9 mW/cm^2) in composition with B-IOD-SbF_6 (3% wag.) compound as the photoinitiator.

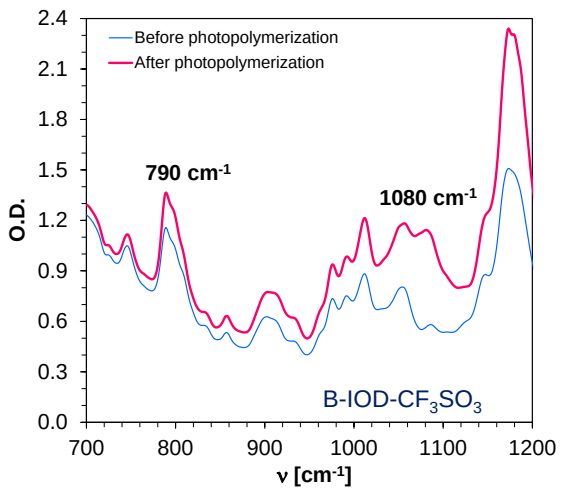

Fig. S69: FT-IR spectra before and after photopolymerization of CADE monomer under Vis-LED 470 nm irradiation (12.9 mW/cm^2) in composition with B-IOD-CF_3SO_3 (3% wag.) compound as the photoinitiator.

Applicability of BODIPY derivatives for on-line monitoring progress of TEGDVE monomer under visible LED 470 nm (12.9 mW/cm^2)

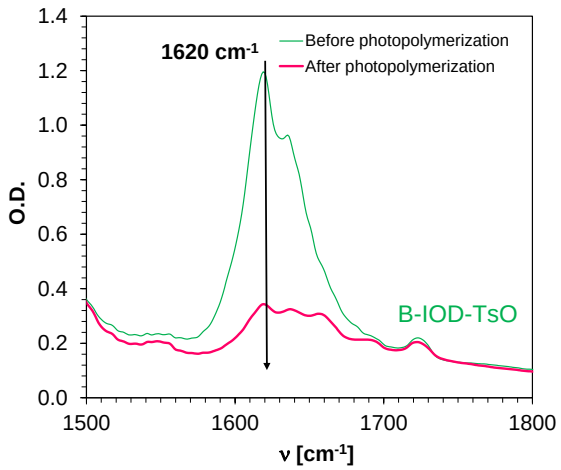

Fig. S70: FT-IR spectra before and after photopolymerization of TEGDVE monomer under Vis-LED 470 nm irradiation (12.9 mW/cm^2) in composition with B-IOD-TsO (3% wag.) compound as the photoinitiator.

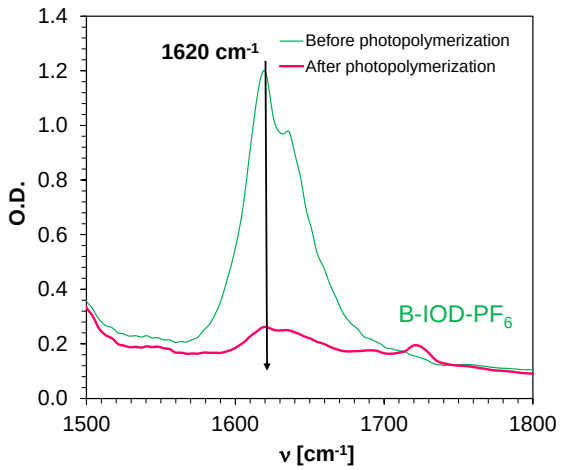

Fig. S71: FT-IR spectra before and after photopolymerization of TEGDVE monomer under Vis-LED 470 nm irradiation (12.9 mW/cm^2) in composition with B-IOD-PF_6 (3% wag.) compound as the photoinitiator.

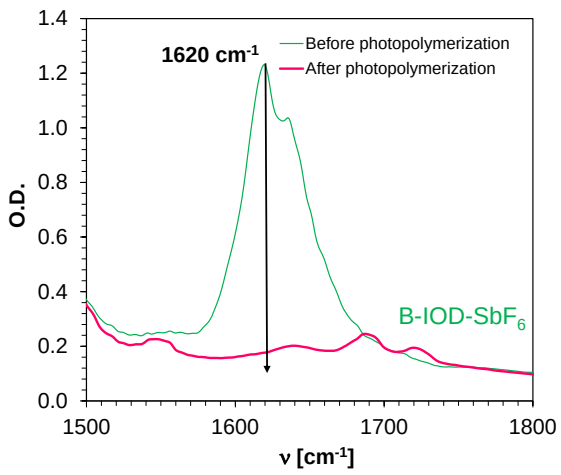

Fig. S72: FT-IR spectra before and after photopolymerization of TEGDVE monomer under Vis-LED 470 nm irradiation (12.9 mW/cm^2) in composition with B-IOD-SbF_6 (3% wag.) compound as the photoinitiator.

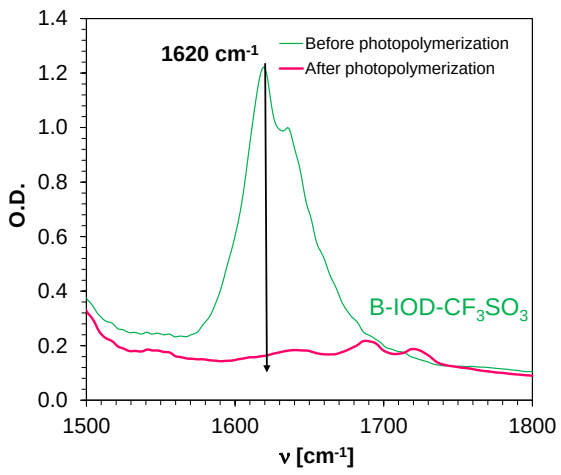

Fig. S73: FT-IR spectra before and after photopolymerization of TEGDVE monomer under Vis-LED 470 nm irradiation (12.9 mW/cm^2) in composition with B-IOD-CF_3SO_3 (3% wag.) compound as the photoinitiator.

Cyclic voltammetry curves showing oxidation and reduction processes of 4,4-difluoro-1,3,5,7,8-pentametylo-4-bora-3a, 4a-diaza-s-indacen in acetonitrile

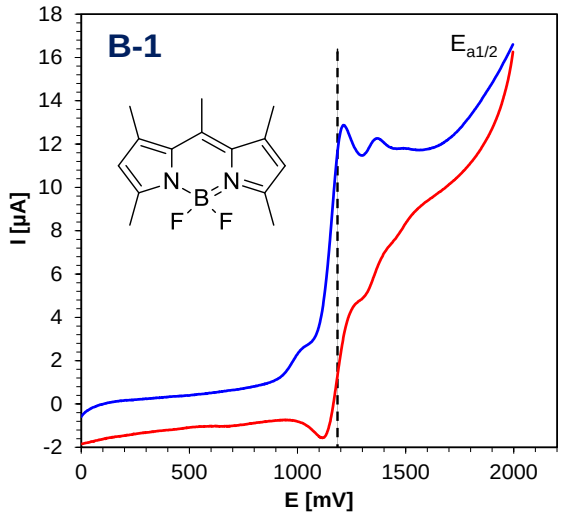

Figure S74: Cyclic voltammogram curves of the 4,4-difluoro-1,3,5,7,8-pentametylo-4-bora-3a, 4a-diaza-s-indacen oxidation in acetonitrile.

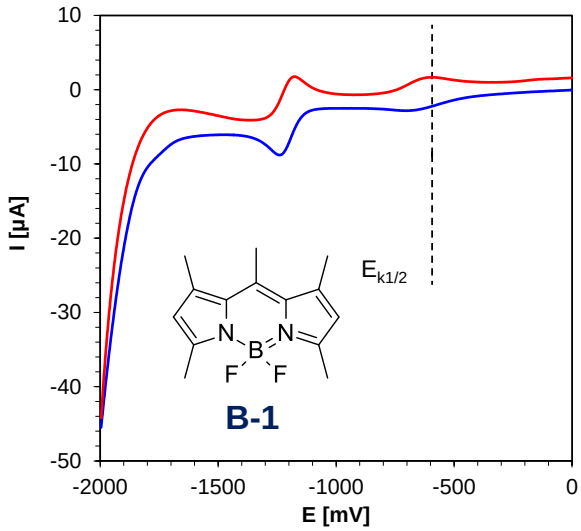

Figure S75: Cyclic voltammogram curves of 4,4-difluoro-1,3,5,7,8-pentametylo-4-bora-3a, 4a-diaza-s-indacen reduction in acetonitrile.

Absorption and fluorescence spectra for the determination of the excited singlet state energy for investigated of 2-amino-4,6-diphenylpyridine-3-carbonitrile derivatives in acetonitrile

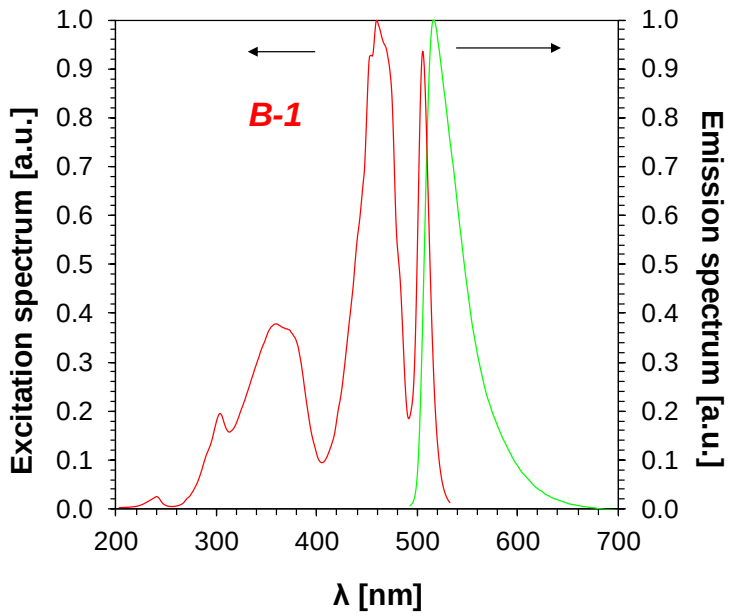

Figure S76: Absorption and fluorescence spectra for the determination of the excited singlet state energy for 4,4-difluoro-1,3,5,7,8-pentametylo-4-bora-3a,4a-diaza-s-indacen .

Fluorescence quenching of B-1 by Speedcure 938 in acetonitrile

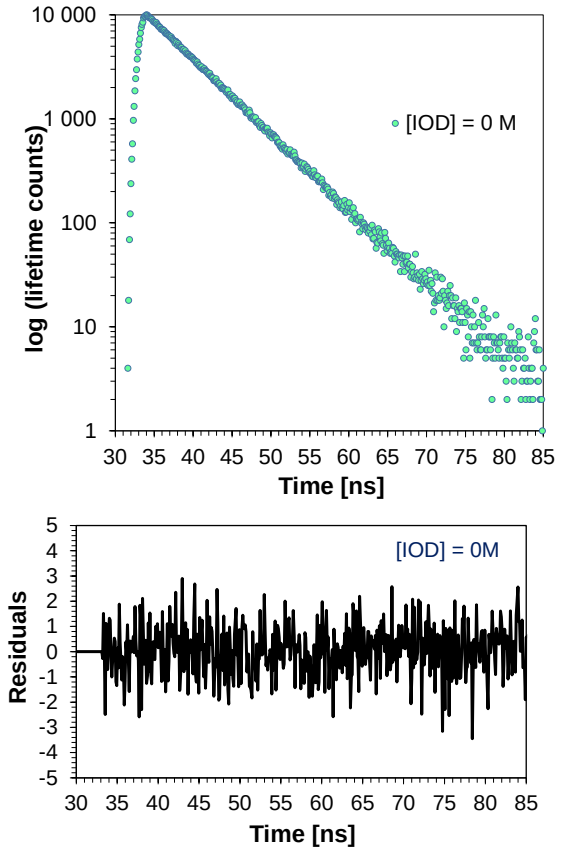

Fig. S77: Dependence of log(lifetime counts) on time for B-1. Random distribution of weighed residual of B-1 and Speedcure 938 (0 M) in acetonitrile.

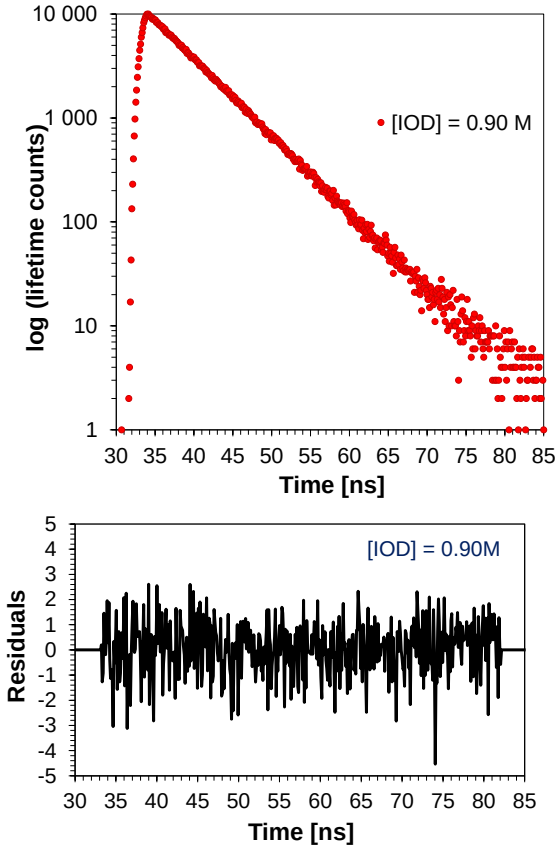

Fig. S78: Dependence of log(lifetime counts) on time for B-1 in presence of Speedcure 938 (0.90M). Random distribution of weighed residual of B-1 and Speedcure 938 (0.90 M) in acetonitrile.

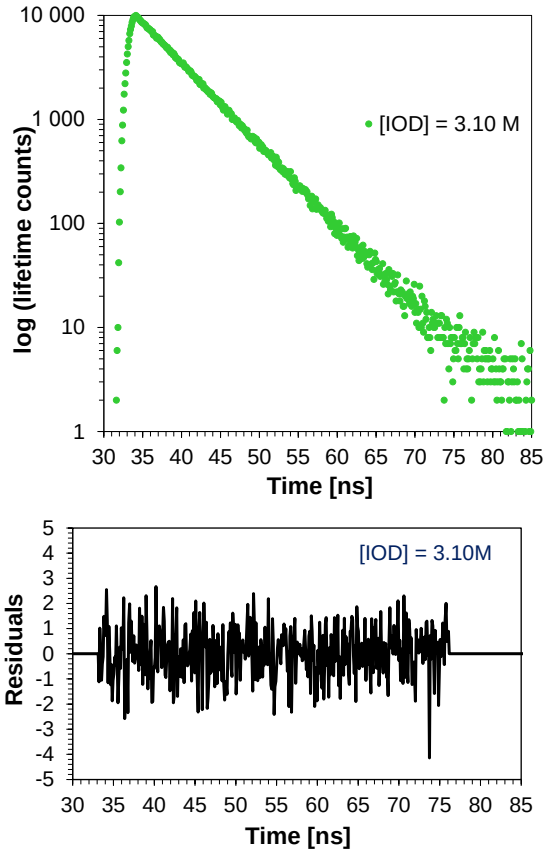

Fig. S79: Dependence of log(lifetime counts) on time for B-1 in presence of Speedcure 938 (3.10M). Random distribution of weighed residual of B-1 and Speedcure 938 (3.10 M) in acetonitrile.

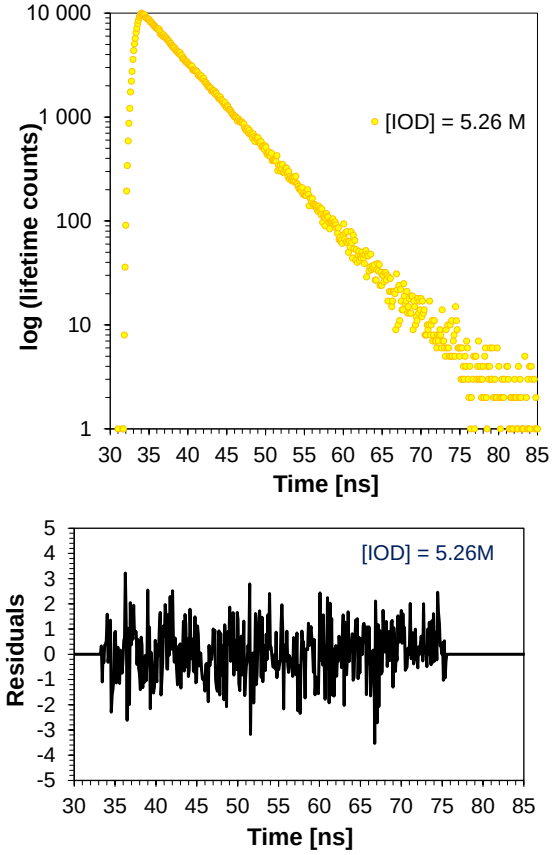

Fig. S80: Dependence of log(lifetime counts) on time for B-1 in presence of Speedcure 938 (5.26M). Random distribution of weighed residual of B-1 and Speedcure 938 (5.26 M) in acetonitrile.

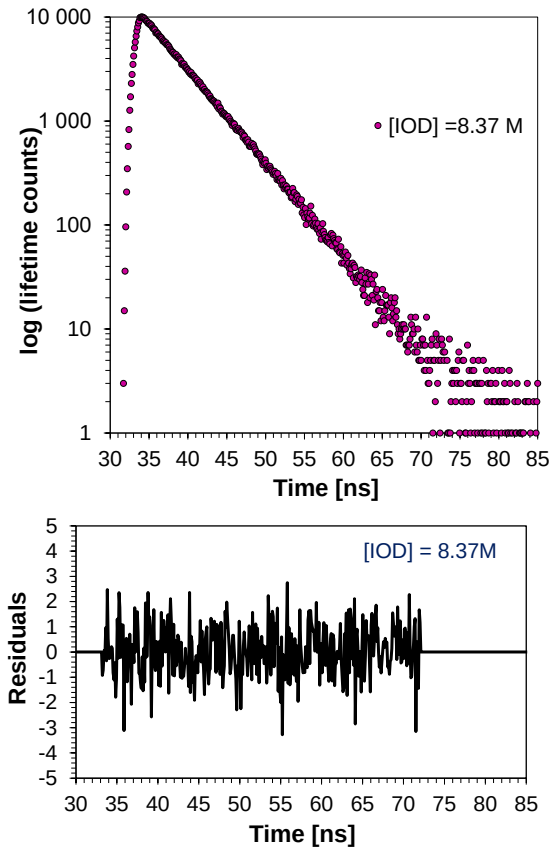

Fig. S81: Dependence of log(lifetime counts) on time for B-1 in presence of Speedcure 938 (8.37M). Random distribution of weighed residual of B-1 and Speedcure 938 (8.37 M) in acetonitrile.

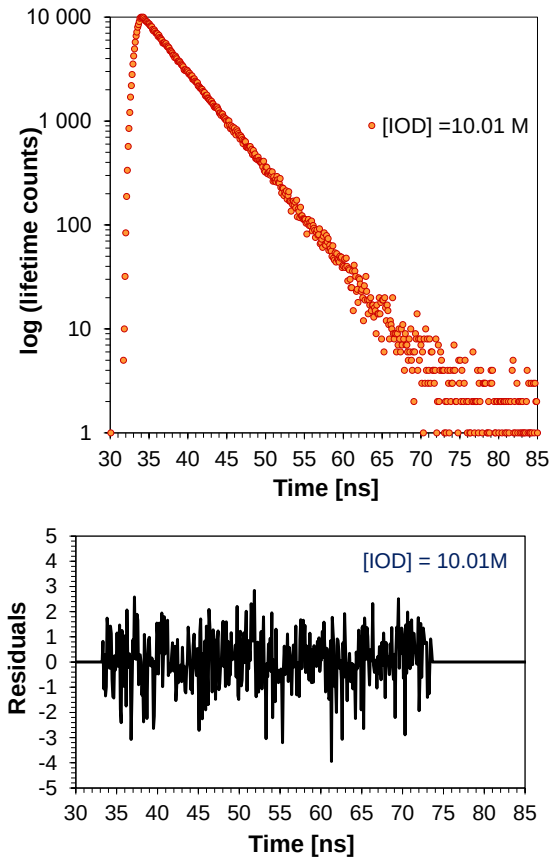

Fig. S82: Dependence of log(lifetime counts) on time for B-1 in presence of Speedcure 938 (10.01M). Random distribution of weighed residual of B-1 and Speedcure 938 (10.01 M) in acetonitrile.

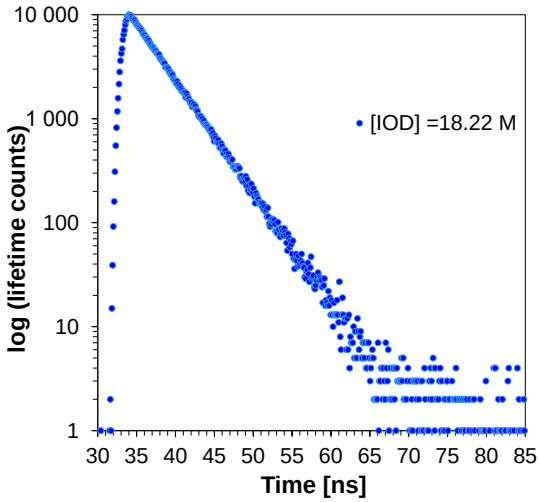

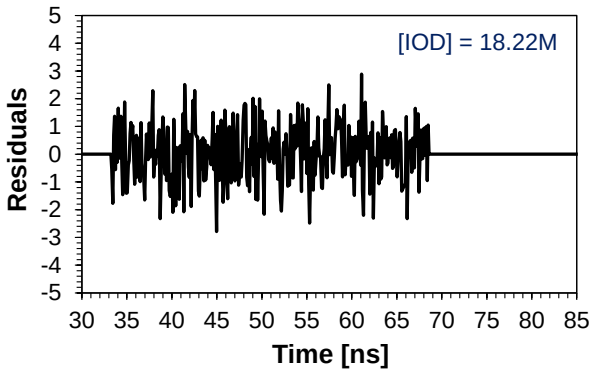

⇐**Fig. S83:** Dependence of log(lifetime counts) on time for B-1 in presence of Speedcure 938 (18.22M). Random distribution of weighed residual of B-1 and Speedcure 938 (18.22 M) in acetonitrile.

Applicability of B-1 and Speedcure 938 for on-line monitoring progress of TEGDVE monomer under visible LED 470 nm (12.9 mW/cm^2)

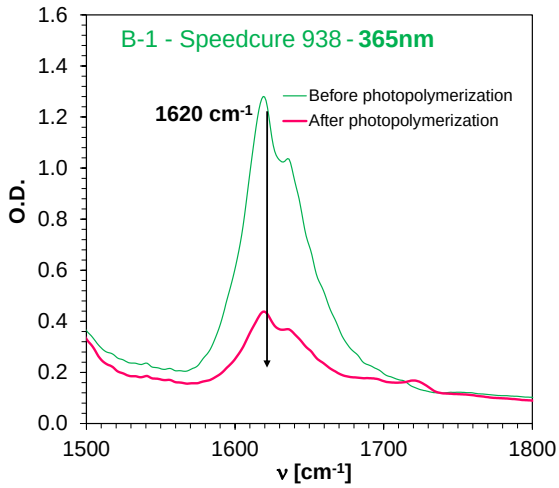

Fig. S84: FT-IR spectra before and after photopolymerization of TEGDVE monomer under UV-LED 365 nm irradiation (12.9 mW/cm^2) in composition with B-1 (0.1%wag.) and Speedcure 938 (1% wag.)

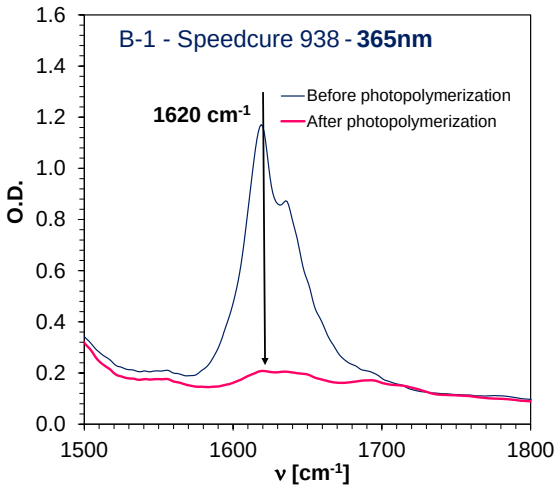

Fig. S85: FT-IR spectra before and after photopolymerization of TEGDVE monomer under UV-LED 365 nm irradiation (12.9 mW/cm^2) in composition with B-1 and Speedcure 938 (1% wag.)

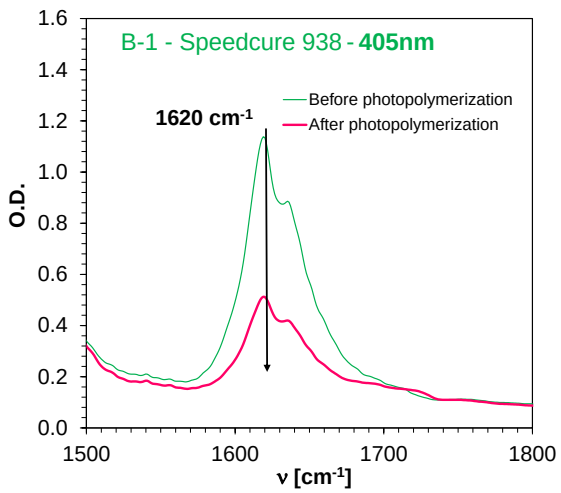

Fig. S86: FT-IR spectra before and after photopolymerization of TEGDVE monomer under Vis-LED 405 nm irradiation (12.9 mW/cm^2) in composition with B-1 (0.1%wag.) and Speedcure 938 (1% wag.).

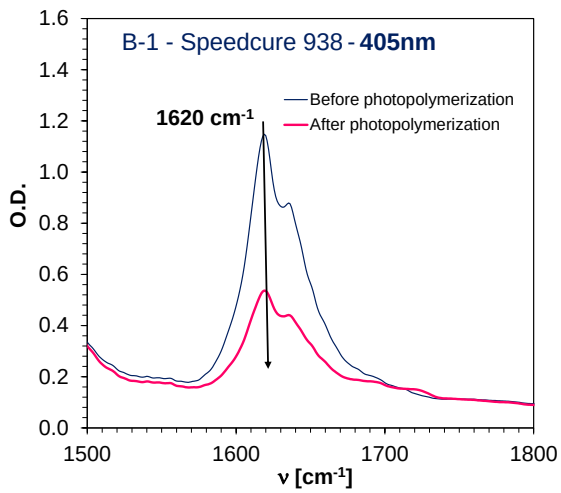

Fig. S87: FT-IR spectra before and after photopolymerization of TEGDVE monomer under Vis-LED 405 nm irradiation (12.9 mW/cm^2) in composition with B-1 and Speedcure 938 (1% wag.)

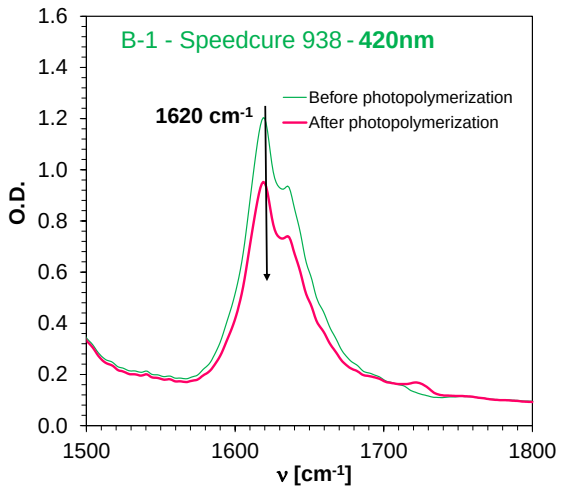

Fig. S88: FT-IR spectra before and after photopolymerization of TEGDVE monomer under Vis-LED 420 nm irradiation (12.9 mW/cm^2) in composition with B-1 (0.1%wag.) and Speedcure 938 (1% wag.).

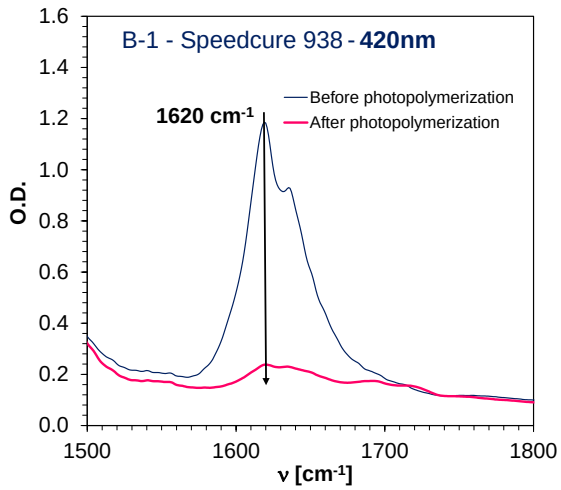

Fig. S89: FT-IR spectra before and after photopolymerization of TEGDVE monomer under Vis-LED 420 nm irradiation (12.9 mW/cm^2) in composition with B-1 and Speedcure 938 (1% wag.).

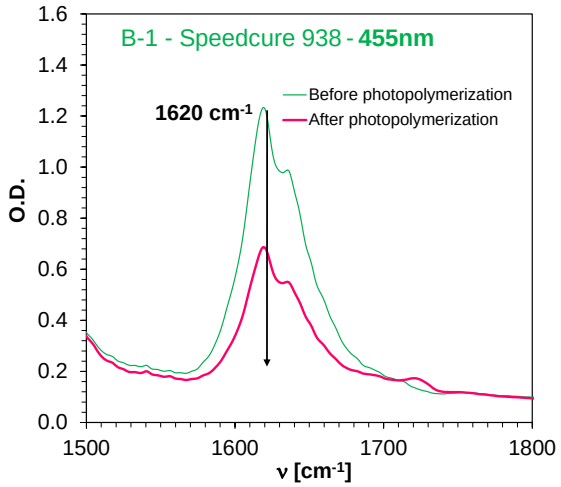

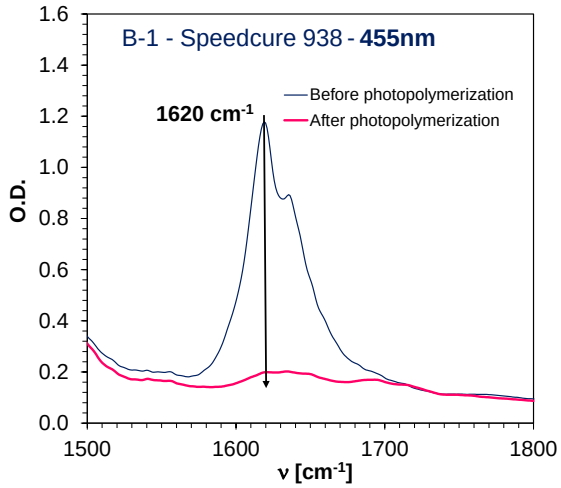

Fig. S90: FT-IR spectra before and after photopolymerization of TEGDVE monomer under Vis-LED 455 nm irradiation (12.9 mW/cm^2) in composition with B-1 (0.1%wag.) and Speedcure 938 (1% wag.).

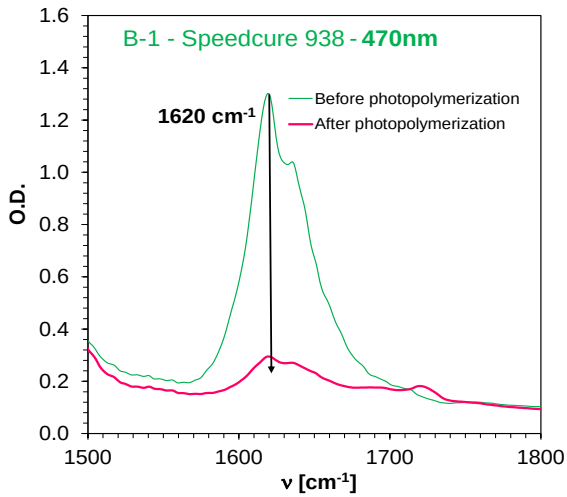

Fig. S91: FT-IR spectra before and after photopolymerization of TEGDVE monomer under Vis-LED 455 nm irradiation (12.9 mW/cm^2) in composition with B-1 and Speedcure 938 (1% wag.).

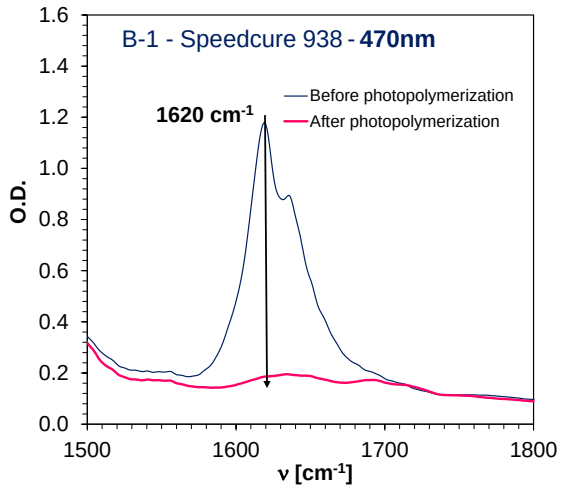

Fig. S92: FT-IR spectra before and after photopolymerization of TEGDVE monomer under Vis-LED 470 nm irradiation (12.9 mW/cm^2) in composition with B-1 (0.1%wag.) and Speedcure 938 (1% wag.).

Fig. S93: FT-IR spectra before and after photopolymerization of TEGDVE monomer under Vis-LED 470 nm irradiation (12.9 mW/cm^2) in composition with B-1 and Speedcure 938 (1% wag.).

Applicability of B-1 and Speedcure 938 and/or EDB for on-line monitoring progress of TMPTA monomer under visible LED 470 nm (12.9 mW/cm^2)

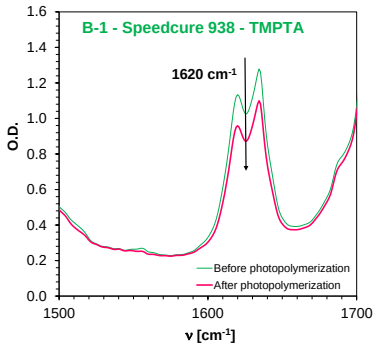

Fig. S94: FT-IR spectra before and after photopolymerization of TMPTA monomer under Vis-LED 470 nm irradiation (12.9 mW/cm^2) in composition with B-1 3%wag.) and Speedcure 938 (1% wag.).

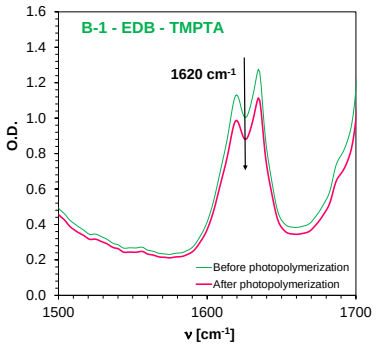

Fig. S95: FT-IR spectra before and after photopolymerization of TMPTA monomer under Vis-LED 470 nm irradiation (12.9 mW/cm^2) in composition with B-1 (0.5%wag.) and EDB (1.5% wag.).

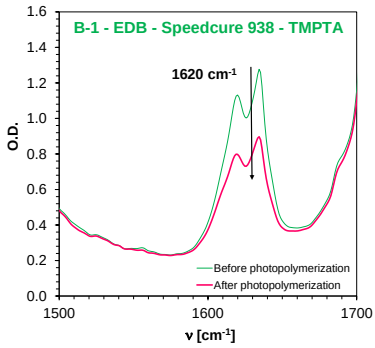

Fig. S96: FT-IR spectra before and after photopolymerization of TMPTA monomer under Vis-LED 470 nm irradiation (12.9 mW/cm^2) in composition with B-1 (0.5%wag.) and Speedcure 938 (1% wag.) and EDB (1.5% wag.).

Laser flash photolysis

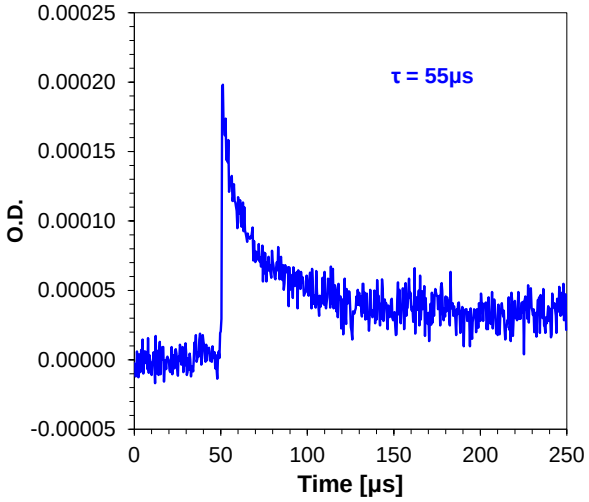

Fig. S97: Transient absorption recorded at 400 nm for a laser excitation at 355 nm for B-1 in nitrogen saturated acetonitrile.

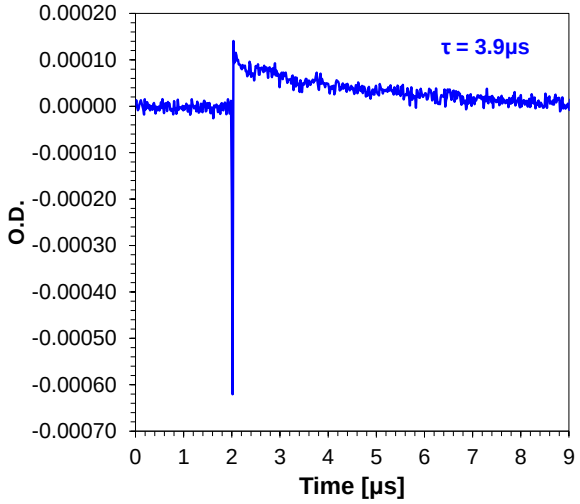

Fig. S98: Transient absorption recorded at 400 nm for a laser excitation at 355 nm for B-IOD-PF_6 in nitrogen saturated acetonitrile.

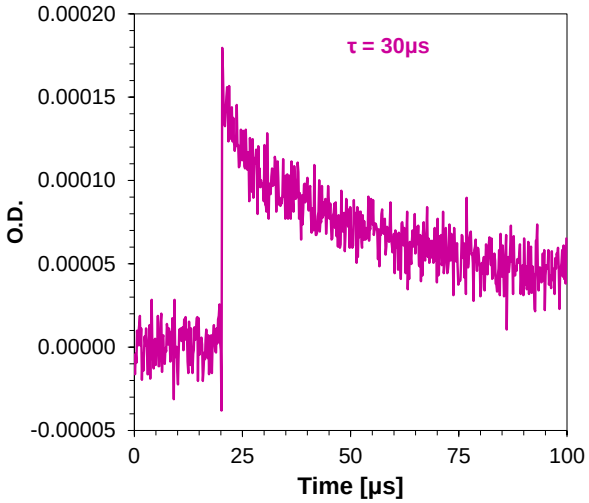

Fig. S99: Transient absorption recorded at 400 nm for a laser excitation at 355 nm for B-1 in oxygen saturated acetonitrile.

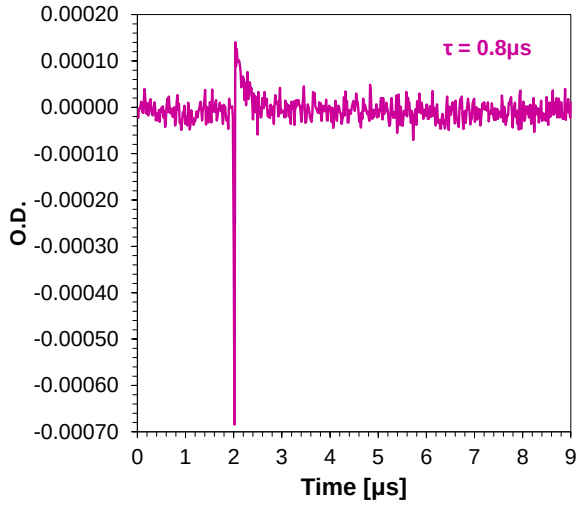

Fig. S100: Transient absorption recorded at 400 nm for a laser excitation at 355 nm for B-IOD-PF_6 in oxygen saturated acetonitrile.

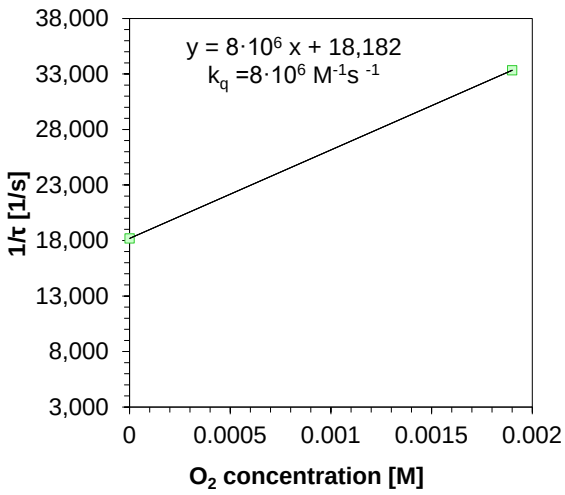

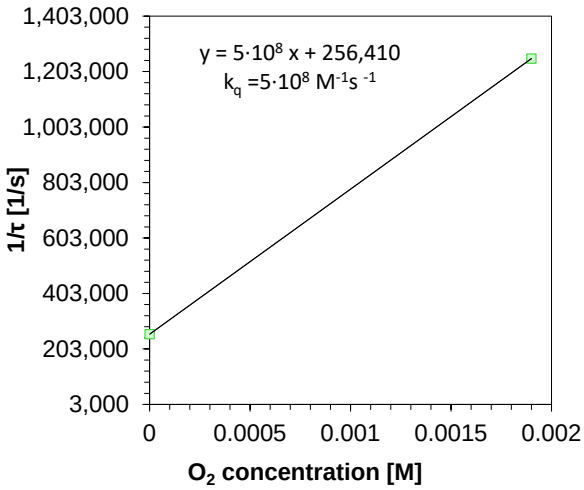

Fig. S101: Dependence 1/τ on O_2 concentration for B-1.

Fig. S102: Dependence 1/τ on O_2 concentration for B-IOD-PF_6.

Absorbance of B-1 and B-IOD-PF_6

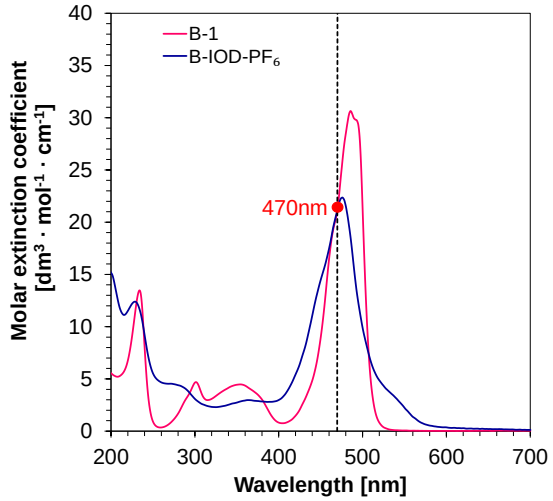

Fig. S103: UV-visible absorption spectra of the B-1 and B-IOD-PF_6 in acetonitrile, the same molar extinction coefficient at the 470nm.

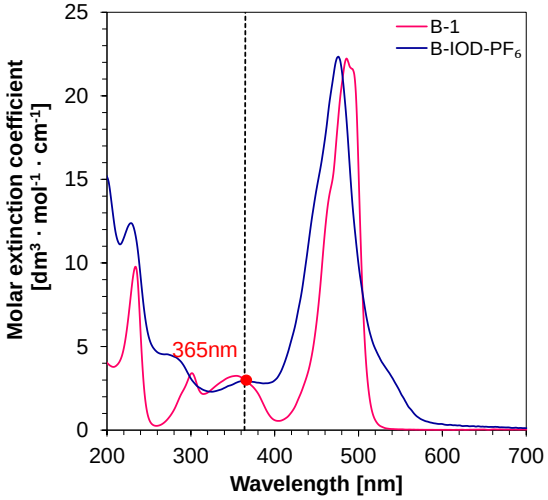

Fig. S104: UV-visible absorption spectra of the B-1 and B-IOD-PF_6 in acetonitrile, the same molar extinction coefficient at the 365nm.

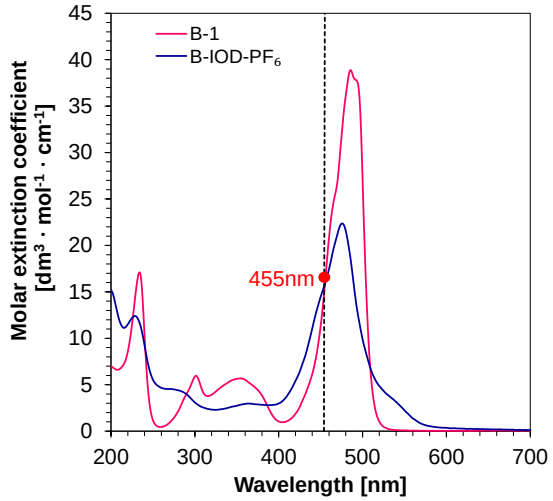

Fig. S105: UV-visible absorption spectra of the B-1 and B-IOD-PF_6 in acetonitrile, the same molar extinction coefficient at the 455nm.

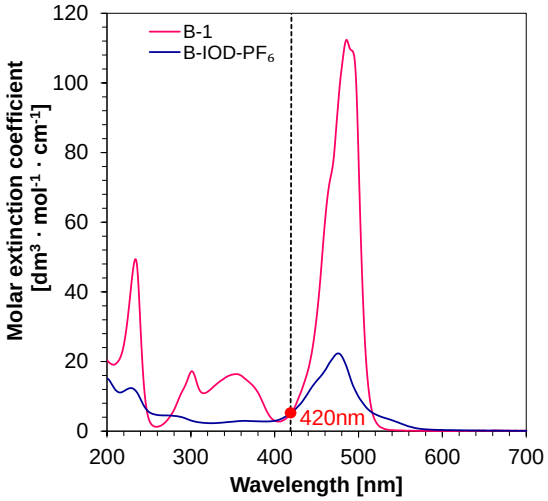

Fig. S106: UV-visible absorption spectra of the B-1 and B-IOD-PF_6 in acetonitrile, the same molar extinction coefficient at the 420nm.

1. M. Topa, M. Galek, J. Ortyl, Nowe sole jodoniowe, sposób ich wytwarzania i zastosowania, Pat.238234